The report indicates the status of a research project that is still ongoing within GIA.
Comments on this and other reports and their direction are warmly welcomed as are offers of collaboration.
Contact information can be found in the "about the authors" section on page 43.

AN IN-DEPTH STUDY OF BLUE SAPPHIRES

FROM PAILIN, CAMBODIA

Sudarat Saeseaw, Supharart Sangsawong, Wim Vertriest, and Ungkhana Atikarnsakul

Figure 1: A parcel of heated blue sapphires reported to have been mined at O Ta Prang area, near Phnum Yat in Pailin and an unheated, trapiche type blue sapphire crystal of the milky type commonly found in Pailin. Photo: Vincent Pardieu © GIA.

Table of Contents

1.1 Location

The Pailin province is located in the western part of Cambodia, near the Thai border. The main city is also called Pailin. The small province is completely surrounded by the Battambang province. In the South the Cardamom mountains form a natural border. The area around Pailin is deforested and converted into farmland for various crops such as maize and cassava. Gem mining is concentrated on the flanks of sapphire producing volcanos, near rivers or in old riverbeds.

Around Pailin, the main volcanic hills that brought sapphires to the surface are:
- Phunm Yat which produces mainly sapphires and is located in the city center.
- Phnum O Tang and Phnum Ko Ngoap which produces mainly ruby and to a lesser degree sapphire. They are located towards the west and northwest of Pailin.
- Phunm Trop has brought ruby and sapphire to the surface in the mountains south of Pailin

Gemstones were also mined around the town of Samlaut, south-east of the mountain range, in current Battambang province.

Figure 2: Map of Pailin region with the main sapphire producing volcanoes.

Phnum Yat holds a great spiritual meaning to the local people. On the top of this hill, a temple was built which clearly shows Burmese influences. The whole hill is considered sacred and has never been mined, although its immediate surroundings have all been dug up in the search for gemstones. On the temple grounds, there is a shrine dedicated to Ye Yat. According to the local legends, she is responsible for the discoveries of gemstones near Pailin. One day a group of hunters was going through the woods covering the flanks of Phnum Yat when they encountered a forest spirit that had taken the form of an old lady. She told the hunters to leave the forest unharmed and go to the river where a new source of income would be revealed to them. When the men reached the river they spotted some otters in the water. The small animals were playing with bright red and blue stones, and thus rubies and sapphires were discovered in Pailin.

Figure 3: Statue of Ye Yat in the temple on Phnum Yat hill. Photo by Vincent Pardieu-GIA.

1.2 History of sapphire mining in Cambodia

Rubies (and sapphires) are mined along the current Thai-Cambodian border for more than a century. The deposit was known for centuries and exploited by Burmese merchants traveling to the Mekong in the 19th century (Ma Huan 1970). Several travelers reported Burmese people searching for gems near Chanthaburi and Pailin in 1880-1896 (Smyth, 1994, Pavie, 1999).

In 1907 the provinces of Battambang, Siem Reap and Sisophon (Present Cambodia) were returned to French Indochina. Pailin and Samlaut, part of the Battambang province, became part of French Indochina. Until this time, up to 90% of the global fine sapphire production was coming from the Cambodian mines.

During the war that devastated the country from 1970 to 1999, Pailin was a Khmer rouge stronghold. In the 70s, most of the mining was halted, but it picked up in the 80s. The Khmer Rouge regime allowed Thai miners to work in Pailin and Samlaut to finance their fight against the Vietnamese. At the time of writing, a few mechanized mining operations are still active around Pailin and artisanal miners can be found mining in the river gravels.


Figure 4: A river miner shows the day's production. Photo by Wim Vertriest-GIA.

1.3 Geology of the Pailin sapphire deposits

1.3.1 OCCURENCE

The gem deposits of Pailin are associated with alkali basalts (Berrangé and Jobbins 1976, Vichit, Vudhichativanich et al. 1978, Jobbins and Berrangé 1981, Keller 1982). These are basalts that form at great depths, usually assumed to be in the mantle, near the transition with the crust. SE-Asia hosts multiple alkali basalt extrusions that are of Cenozoic (Tertiary) age. Although most of them are not gem bearing or are rich enough to be commercially exploited, some of these deposits have had a serious impact on the global gemstone trade (Bo Ploi, Chanthaburi-Trat, and Pailin) (figure 5).
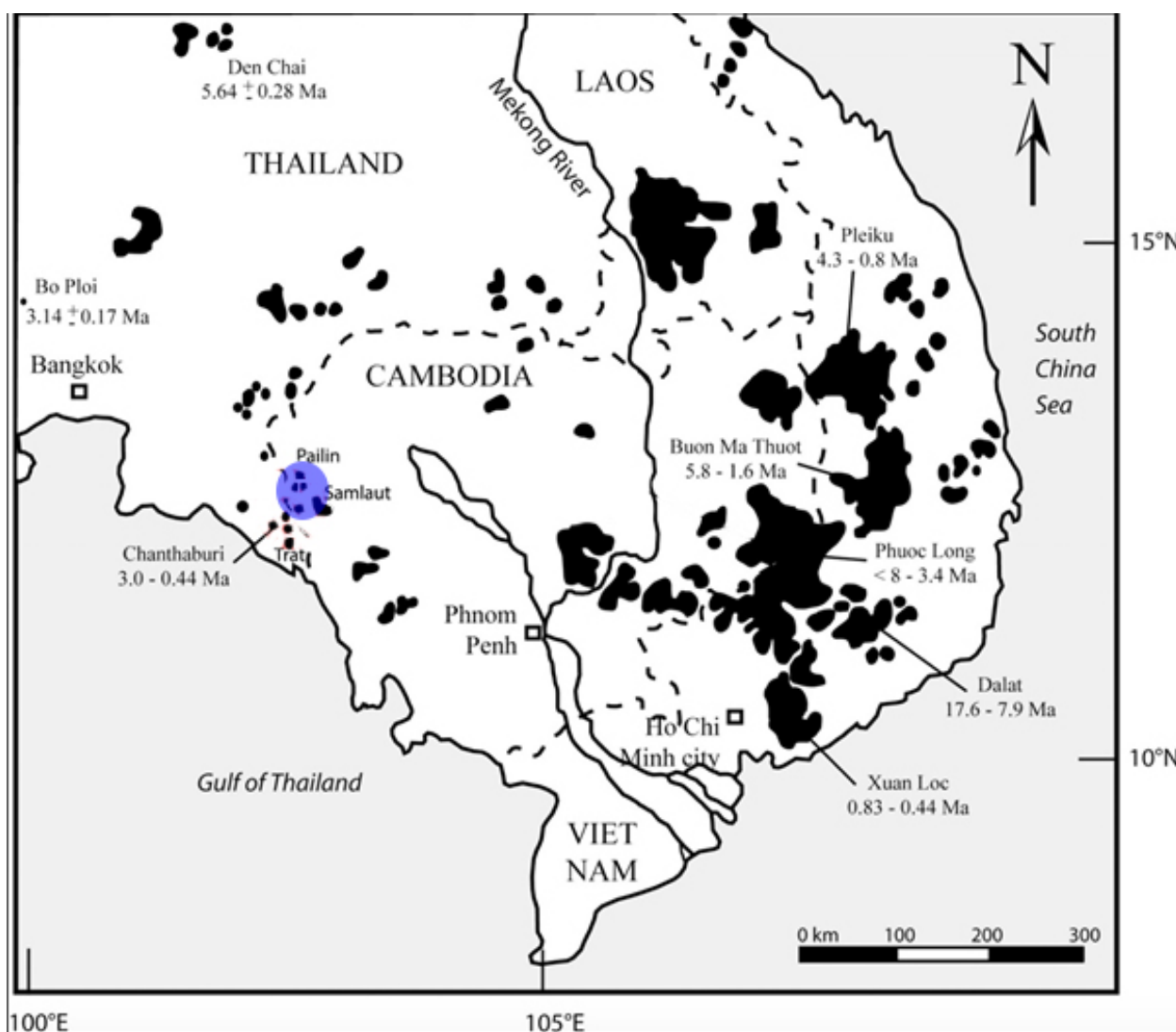
Figure 5: Map of the different basalt fields in South East Asia with their respective ages. The area highlighted in blue is where most of the Cambodian sapphires are mined. Modified from Garnier et al, 2001

Due to South-East Asia's hot and humid climate, the alkali-basalt weathers very quickly. During the weathering process, the more stable minerals are liberated from their basalt matrix. These are mainly corundum, garnet, zircon and large clinopyroxenes. The basalt matrix, which consists of finer-grained pyroxenes, is turned into a reddish mud (Keller 1982).

The released gemstones are found in secondary, alluvial deposits. These river deposits can concentrate heavy minerals in certain locations where the river's energy and speed is lower. These traps are found behind large boulders, in river curves and after river-sections containing rapids.

In the river deposits around Pailin, these traps contain minerals associated with the alkali basalts, but also heavy minerals from other rocks found nearby. Examples are gold and several garnet varieties, which are also found by the miners working recent and paleo-river deposits.

1.3.2 GENESIS OF THE CORUNDUM

Basalt-related gems have been extensively studied and it is accepted that the corundum is a xenocryst in the igneous rocks. This means that the corundum was not formed in the basalt, but was picked up at depth when the magma was travelling to the surface. In the literature a few arguments are commonly used to prove that the sapphires are xenocrysts (Levinson and Cook 1994, Sutherland, Hoskin et al. 1998, Saminpanya and Sutherland 2011)

- The corundum never shows a perfect crystal habit, it is always rounded (even when found in the basalt) and shows etching and resorption, indicating the basalt has started to consume or dissolve the corundum because it is unstable in the basalt during emplacement.
- Several inclusions in basalt-related rubies and sapphires are impossible to form in alkali basalts.

The first experiments to crystallize corundum from an experimental melt with composition similar to alkali basalt were unsuccessful (Levinson and Cook 1994), but more recent work has yielded positive results. An experiment has found corundum as inclusions in garnets formed during the crystallization of alkali basalt at high pressure and temperature. The process is not well understood and is assumed to be highly complex. However, this experiments shows that it might be possible to crystallize corundum megacrysts directly out of an alkali basalt (Hong-sen, Wei-guo et al. 2002).
Although this publication shows that it is theoretically possible for alkali basalt to crystallize corundum, it is still assumed that corundum is a xenocryst in alkali basalt.

The exact genesis of this corundum is still under debate, and several theories have been formed.
A short literature review is given here:

- Corundum crystallized in plutonic bodies of syentic composition. These bodies formed in the lower crust to upper mantle (Aspen, Upton et al. 1990)
- Sapphire formed in alkaline Si-Al rich melts that evolved from basaltic magmas (Coenraads, Sutherland et al. 1990, Coenraads 1992)
- Corundum formed in subducted Al-rich rocks that metamorphosed under high pressure and temperatures (Levinson and Cook 1994)

- Sapphire formed in alkaline Si-Al rich melts. These melts are derived from the partial melting of metasomatised mantle (Sutherland 1996).
- Sapphires formed in reaction zones between Si-rich and carbonatitic magmas at mid-crustal levels. The conditions are around 400 °C and depths of 10-20 km (Guo, O'Reilly et al. 1996)
- Sapphire formation is linked to melting of amphibole-bearing source rocks near the crust-mantle boundary. This forms magmas with high Al concentration which lead to corundum formation (Sutherland, Schwarz et al. 1998)
- Sapphires formed in a carbonatitic (CO_2 rich) melt that fractionated from the alkali basalt (Baldwin, Tomaschek et al. 2017).

All these models formulate a hypothesis on how corundum formed in the earth before it was carried to the surface. Up to now, no agreed-upon model has been developed.
Studying the geology of basalt-related corundum is extremely complicated due to the limited amount of samples in basalt-matrix that are available. Finding xenoliths which contain fragments corundum and the original mother-rock will shine a new light on the formation of these gems, but such samples are nearly unheard of.

1.4 Mining techniques

Several types of ruby-mining operations can be found in the area west of Pailin. The first type works in old riverbeds and operates on the largest scales. These often work with machines including jigs, pumps and excavators. The excavators are used to remove large blocks. Pumps and high-pressure waterjets are used to loosen the finer gravels and muds. Once released, they flow towards a gravel pump. This pump transports the slurry to a mechanized jig where the heavy minerals are concentrated. At the end of the day, the jig is cleared of all valuable stones.

Figure 6: Mining old river deposits near the Pailin River. From bottom to top, we can see: Miner working high pressure waterjet to loosen the gravels; gravel pump to move the slurry; jig to concentrate the minerals. Photo by Vincent Pardieu-GIA.

Other miners work in the active riverbed. The Pailin River has strongly fluctuating levels and has its origins in the Cardamom Mountains, south of Pailin. This mountainous forested area hosts several alkali basalt exposures that produce rubies and sapphires. These are transported during the rainy season. When water levels fall, many traps in the riverbed become accessible and miners start manually washing and sieving the gravels that build up behind big boulders or in river bends.

Figure 7: A Cambodian miner working in the Pailin River during the dry season. In the background are the Cardamom Mountains, which contain several gem-hosting basalts. Photo by Wim Vertriest-GIA.

Figure 8: A miner using a long shovel to get gravel from the river bottom. Photo by Wim Vertriest-GIA.

Figure 9: A miner removing the oversized material from his washing screen. Photo by Wim Vertriest-GIA.

Some miners decided to create artificial traps by digging holes in the river bed. When the water levels rise, these holes trap heavy minerals. The next year, when the river level has fallen again, they clean the trapped gravels.

Figure 10: Miners create circular pits in the river to form artificial gemstone traps. Apart from mining, kids use them as swimming pools. Photo by Wim Vertriest-GIA.

PART II: MATERIALS AND METHODS

2.1 Sample selection and fabrication:

We studied sixty eight (68) samples to characterize features in blue sapphires from Pailin, Cambodia. All samples were collected from different mining sites around Pailin by GIA field gemologists. The field expeditions took place from 2010 to 2017. According to the GIA Field Gemology sample classification system, these samples are type B, C and D-type.

- B-type: Mining was witnessed by the gemologist, usually collected from the jig.
- C-type: Sample was collected from the miner at the mine, but without witnessing the mining.
- D-type: Sample was collected from the miner, but not at the mine (e.g. at the miner's house).

Most of the studied samples have **blue** color when viewed perpendicular to the c-axis direction, which is only the ordinary ray direction (o-ray), whereas **greenish blue** color is seen when viewed parallel to the c-axis direction, which is ordinary and extraordinary ray direction (e-ray). Samples were fabricated for two different purposes:

i) Nine (9) samples that had sufficiently clean areas were fabricated with windows parallel to c-axis for UV-Vis-NIR spectroscopy and chemistry, Table 1.

ii) Fifty-nine (59) samples were fabricated with at two windows for inclusion photography, FTIR, and chemistry, Figure 12.

Figure 11: GIA field gemology team negotiating for gemstone samples with some river miners near Pailin, Cambodia. Photo by Wim Vertriest-GIA.

Table 1: Details of the two sapphires from Pailin, Cambodia selected for UV-Vis-NIR and FTIR spectroscopy, and chemical analysis.

GIA Reference #	Wafer Plane orientation	Wafer path length (mm.)	Image O+E ray	Image through a dichroscope
668918602	Parallel to the C-axis	1.036		Blue/Greenish blue
1003051 62389	Parallel to the C-axis	2.796		Blue/Greenish blue
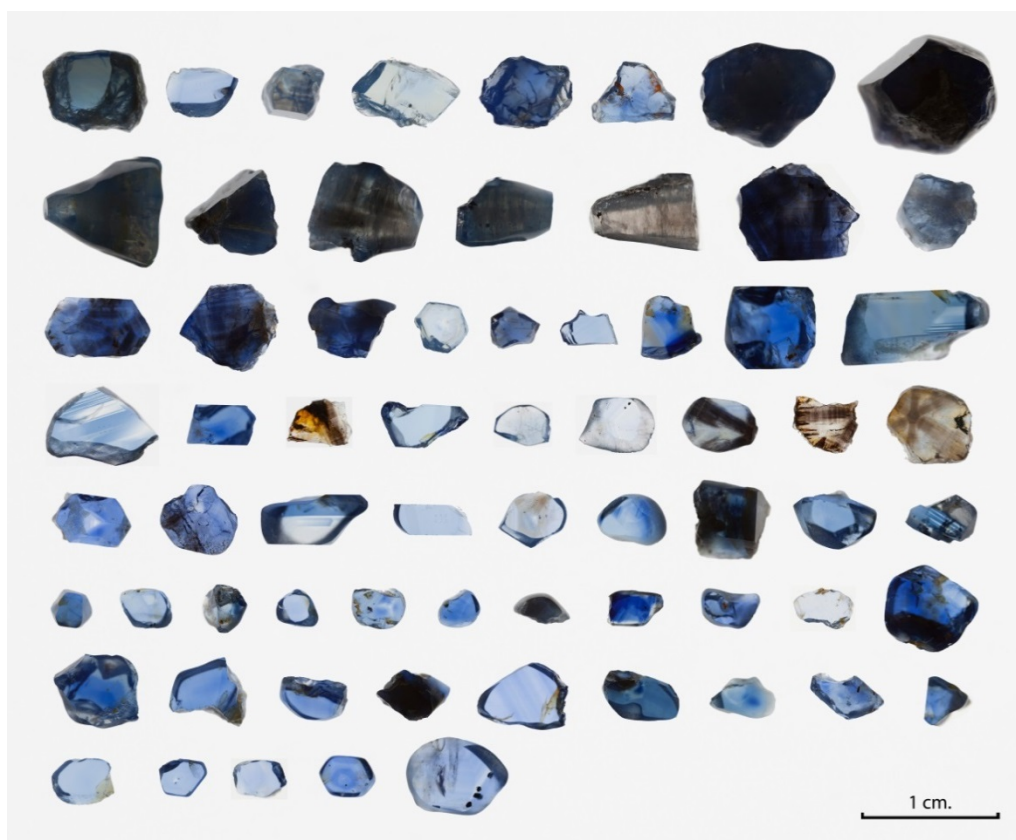
Figure 12: Sixty eight (68) sapphires from Pailin, Cambodia. Translucent samples are Trapiche-like. The photos were color calibrated using transmitted light. Photos: S. Engniwat © GIA.

2.2 Instrumentation:

2.2.1 SAMPLE PHOTOGRAPHY

A Canon EOS 5D camera, with a Canon Macro MP-E 65 mm lens adapted to a camera stand, was used to document the color of the samples. In order to produce consistent results for each sample, the photographs were taken under exactly the same lighting conditions, with the reference samples being placed in a Logan Electric Tru-View 810 Color Corrected Light Box (5000 K lamp). A neutral density filter was used to calibrate the camera light box combination to produce a neutral gray. High-resolution reference photographs were then collected using transmitted light. The color of the sample with polarizer aligned perpendicular to c-axis or 0° sample is the color produced by the O-ray only whereas sample with polarized aligned parallel to c-axis direction or 90° sample is the color produced by both O + E-ray. Photomicrographs of internal features were captured at different magnifications with a Nikon SMZ 18 system and a Nikon SMZ 1500 system using dark field, bright field, diffused and oblique illumination, together with a fiber-optic light source when necessary. It should be noted that magnification power of the microscope was taken into consideration when calculating the field of view (FOV) information in the captions.

2.2.2 UV-VIS-NIR SPECTROSCOPY

Ultraviolet-visible-near infrared (UV-Vis-NIR) spectra were collected with a Hitachi U-2910 spectrophotometer specially modified at GIA to include a rotatable polarizer to allow the separate collection of both the ordinary (O-) and extraordinary (E-) rays. A wavelength resolution of 1.5 nm was used. The spectra obtained were corrected by calculating the reflection loss from the index of refraction data and the data was converted to show their absorption coefficients (α,cm^{-1}) using $\alpha = 2.303A/d$, where A is absorbance and d is the path length in centimeters.

2.2.3 FOURIER TRANSFORM INFRARED ABSORPTION (FTIR) SPECTROSCOPY

FTIR spectroscopy was performed using a Thermo Nicolet 6700 FTIR spectrometer equipped with an XT-KBr beam splitter and a mercury-cadmium-telluride (MCT) detector operating with a 4× beam condenser accessory. Resolution was set at 4 cm^{-1} with 1.928 cm^{-1} data spacing. The spectra obtained were converted to be absorption coefficients (α, cm^{-1}) using $\alpha = 2.303A/d$.

2.2.4 RAMAN SPECTROSCOPY

To identify mineral inclusions, Raman spectra were obtained using a Renishaw inVia Raman microscope fitted with a 514 nm argon-ion laser. The spectra were collected in the range of 100 to 1500 cm^{-1}. At least 5 spectra were collected and stacked until the signal to noise ratio of the spectra was adequate. The calibration was performed using the 520.5 cm^{-1} line of a silicon wafer. In all cases, the RRUFF database (http://rruff.info/) was used as a reference when identifying inclusions. Spectral comparisons were performed using Renishaw Wire (version 3.4) and/or Thermo Galactic 'Spectra ID' (version 3.02) software.

2.2.5 LASER ABLATION-INDUCTIVELY COUPLED PLASMA-MASS SPECTROMETRY (LA-ICP-MS)

Chemical analysis was carried out using LA-ICP-MS technology with a Thermo Fisher Scientific iCAP Q Induced Coupled Plasma-Mass Spectrometer (ICP-MS) coupled with a Q-switched Nd:YAG laser ablation (LA) device operating at a wavelength of 213 nm. Laser conditions used were 55 μm diameter laser spots, a fluence of around 10 J/cm^2, and a 15 Hz repetition rate. Twelve spots were analyzed on each wafer. ICP-MS was operated using the forward power at ~ 1350 W and the typical nebulizer gas flow at ~ 1.00 L/min. Helium was used as the carrier gas in the laser ablation unit and the flow rate was set at ~ 0.60 L/min. The criteria for the alignment and tuning sequence were to maximize Be counts and to keep the ThO/Th ratio below 2%. A special set of doped synthetic corundum standards including Be, Mg, Ti, V, Cr, Fe, and Ga were used for quantitative analysis. All elemental measurements were normalized to Al as the internal elemental standard, (Al=529,200 ppmw). This value approximates to the chemical composition of corundum.

PART III: RESULTS AND DISCUSSION

Sapphires from Pailin, Cambodia have a blue color. Samples showed the standard gemological properties for sapphire with RI-1.760 to 1.770 and were inert both under longwave and shortwave UV radiation.

## 3.1 The internal world of blue sapphires from Pailin, Cambodia

Under microscope examination, blue sapphires from Pailin revealed hexagonal or angular growth features associated with fine-grained or 'milky' clouds. Milky clouds or bands occur in weak (figures 13 to 18) or dense patterns (figures 19 to 21). Dense milky clouds related to rutile particles show as brownish zones using diffused illumination. A few samples contained strong blue color zoning (figures 25 and 26) and bands of minute particles (figures 33 and 34). Intersecting growth tubes along twinning were common in some samples (figures 28 and 29). Stringers of minute particles running across milky bands, along with different crystals such as feldspar, pyrochlore connected with stringers or comet tail like inclusions were also present (figures 49, 51 and 52). Naturally-healed fractures with colorful iridescence, sometimes with angular or hexagonal holes are typically seen in basalt-hosted blue sapphires (figure 41). Two stones displayed streamers or flake-like inclusions (figures 31, 35 and 36). Several crystals were observed in Pailin sapphires including orangy-red pyrochlore, plagioclase feldspar, ferrocolumbite, goethite, zircon, and monazite. They were often associated with decrepitation haloes.
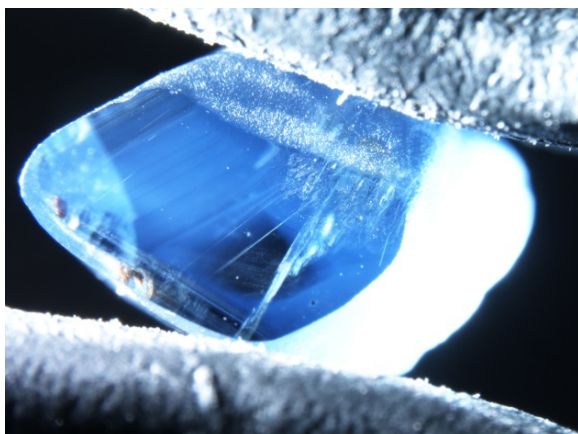
Figure 13: Fine-grained cloud and natural healed fracture in GIA sample #9199 using fiber-optic illumination. FOV 8.2 mm. Photo: C. Khowpong© GIA.
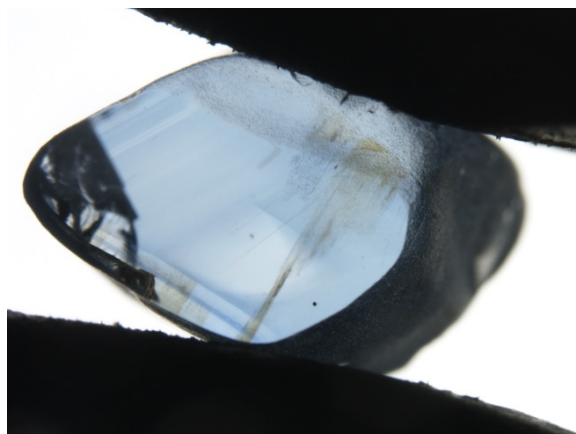

Figure 14: Blue color zoning viewed under diffused illumination in GIA sample #9199. FOV 8.2 mm. Photo: C. Khowpong© GIA.
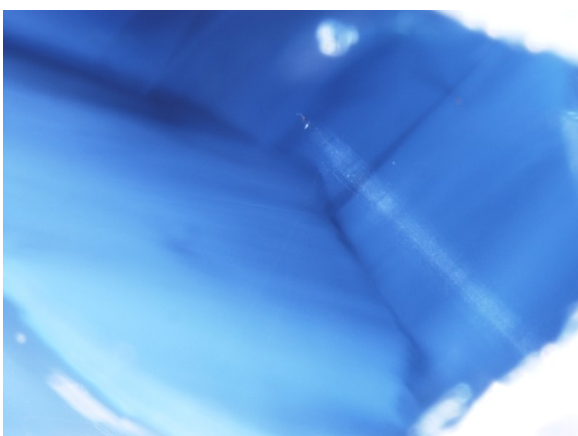
Figure 15: GIA sample #2389 shows very fine grained clouds and stringers of particles using fiber-optic illumination. FOV 2.5 mm. Photo: J. Muyal© GIA.

Figure 16: Under brightfield illumination, strong angular growth features are associated with a fine grained cloud showing brownish zoning in GIA sample #2389. FOV 2.5 mm. Photo: J. Muyal© GIA.
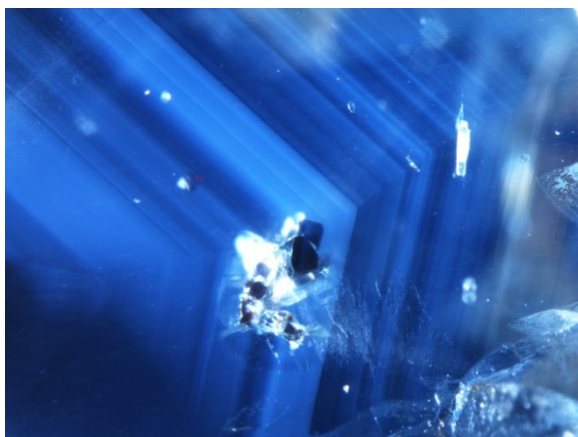
Figure 17: Angular milky banding and opaque crystals in GIA sample #9203 viewed using fiber-optic illumination. FOV 2.0 mm. Photo: C. Khowpong © GIA.
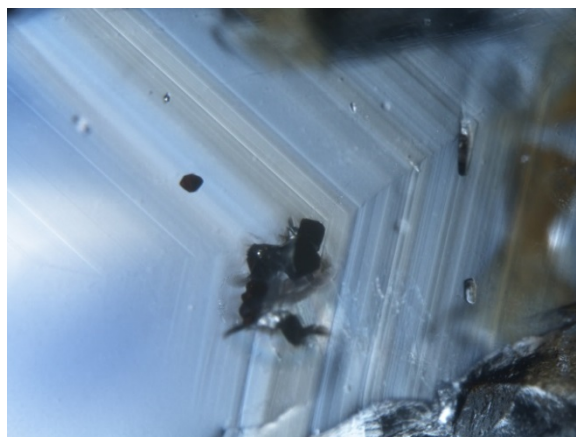
Figure 18: Blue and brownish zones in GIA sample #9203 viewed under brightfield illumination. FOV 2.0 mm. Photo: C. Khowpong © GIA.
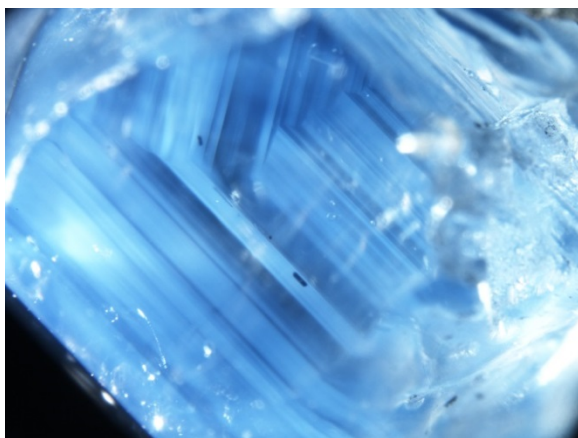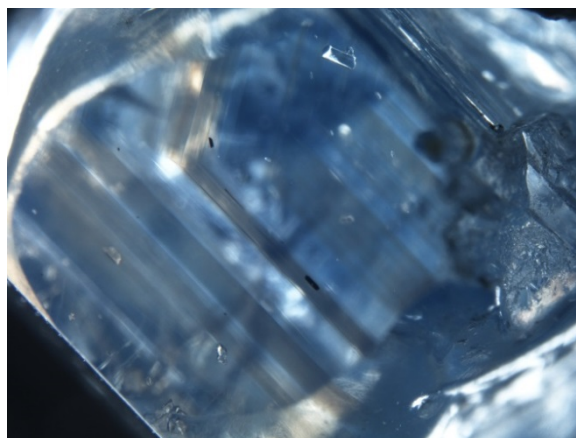
Figure 19: Angular internal growth associated with fine grained clouds in GIA sample #1942 using fiber-optic illumination. FOV 4.0 mm. Photo: C. Khowpong © GIA.

Figure 20: Brownish zoning is clearly seen in fine-grained cloudy areas. Darkfield illumination, GIA sample #1942. FOV 4.0 mm. Photo: C. Khowpong © GIA.
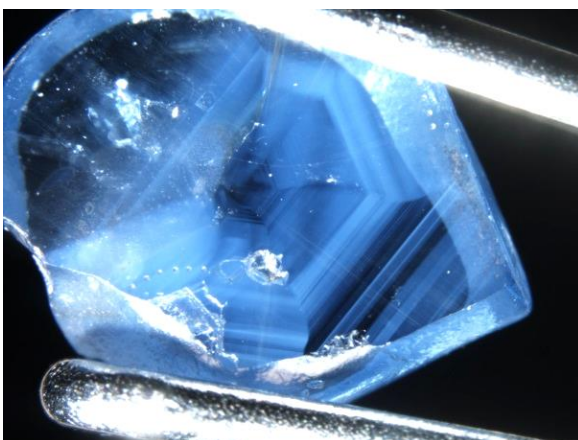
Figure 21: Hexagonal internal growth associated with fine grained clouds in GIA sample #7183. Darkfield and fiber-optic illumination. FOV 6.1 mm. Photo: S. Sangsawong © GIA.

Figure 22: Under diffused illumination, the fine-grained cloudy areas show brownish zoning in GIA sample #7183. FOV 6.1 mm. Photo: S. Sangsawong © GIA.

Figure 23: Hexagonal fine grained cloud associated with internal growth features and naturally-healed fractures in GIA sample #7132 using darkfield illumination. FOV 2.5 mm. Photo: J. Muyal © GIA.
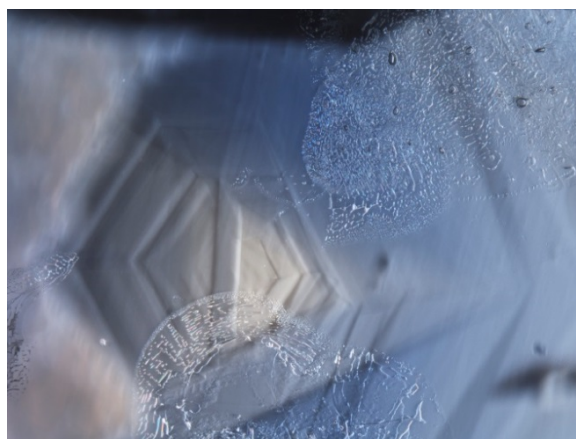
Figure 24: In brightfield illumination, hexagonal growth features with a near colorless core are clearly observed in GIA sample #7132. FOV 2.5 mm. Photo: J. Muyal © GIA.

Figure 25: Strong blue color zoning in GIA sample #2388 viewed using diffused illumination. FOV 9.4 mm. Photo: J. Muyal © GIA.
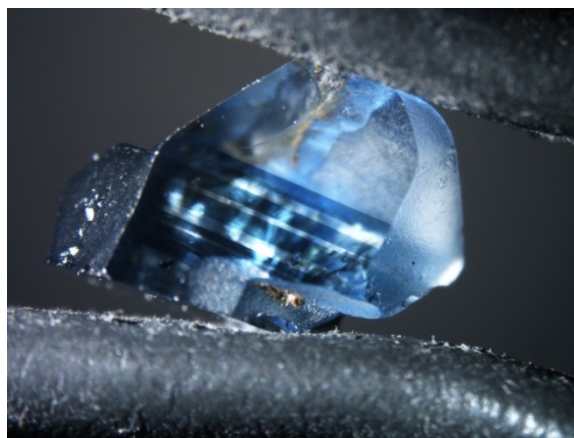
Figure 26: Strong blue color zoning in GIA sample #9197 viewed using fiber-optic illumination. FOV 8.2 mm. Photo: C. Khowpong © GIA.
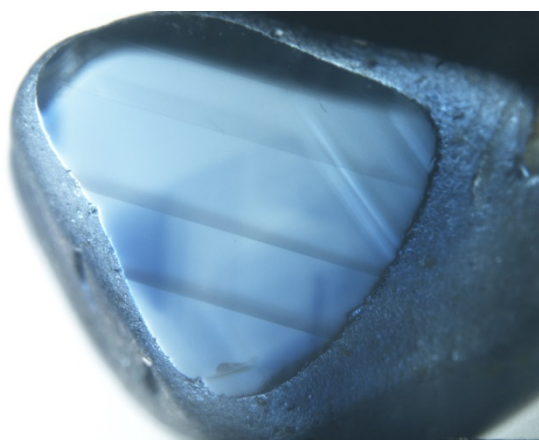
Figure 27: Lamellar twinning in GIA sample #9194 under cross polarizing filters. FOV 8.2 mm. Photo: C. Khowpong © GIA.
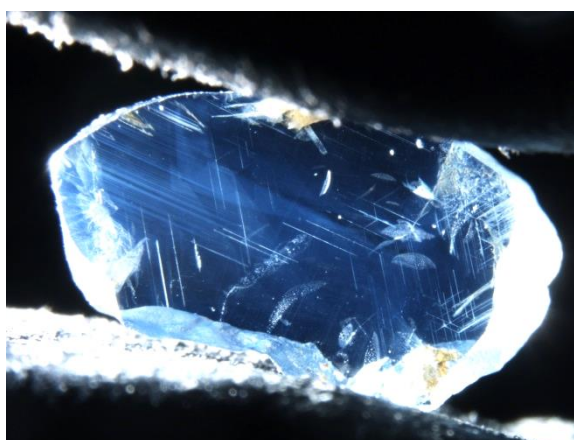
Figure 28: Three intersecting growth tubes along twinning in GIA sample #9208 using fiber-optic illumination. FOV 8.2 mm. Photo: C. Khowpong © GIA.

Figure 29: Three intersecting growth tubes along twinning and angular milk bands in GIA sample #2390. Dark field and fiber-optic illumination. FOV 2.7 mm. Photo: C. Khowpong © GIA.
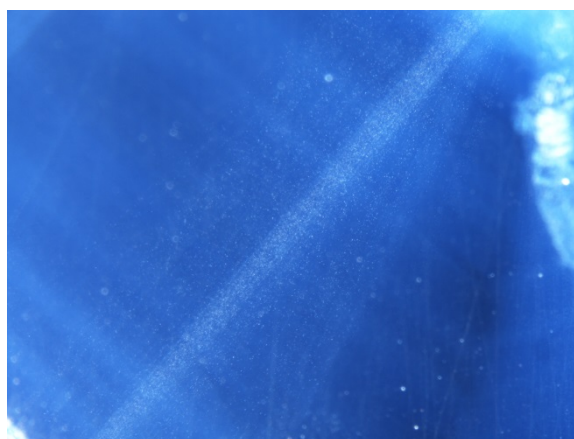
Figure 30: Stringers across milky bands in GIA sample #9212. Fiber-optic illumination. FOV 2.7 mm. Photo: C. Khowpong © GIA.
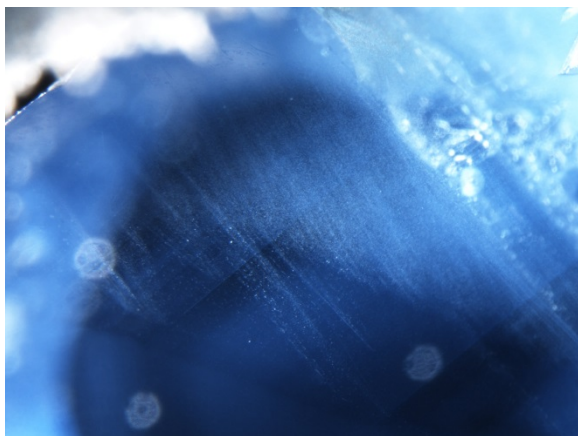
Figure 31: Streamers in GIA sample #9202. Fiber-optic illumination. FOV 2.0 mm. Photo: C. Khowpong © GIA.

Figure 32: Milky cloud, void like inclusions, and stringers in GIA sample #8502. Darkfield and fiber-optic illumination. FOV 1.7 mm. Photo: J. Muyal © GIA.
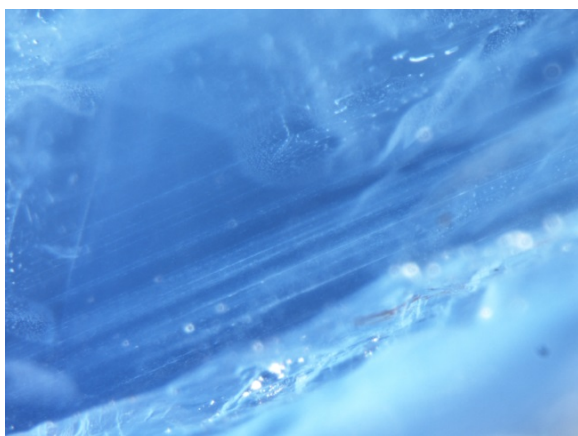
Figure 33: Weak bands of minute particles in GIA sample #2390 are rarely seen in Pailin sapphire. Darkfield and fiber-optic illumination. FOV 0.8 mm. Photo: C. Khowpong © GIA.
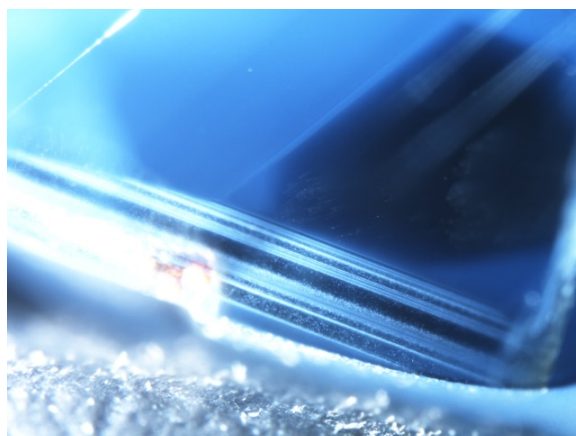
Figure 34: A fine grained cloud and bands of minute particles in GIA sample #9199. Fiber-optic illumination. FOV 2.0 mm. Photo: C. Khowpong © GIA.
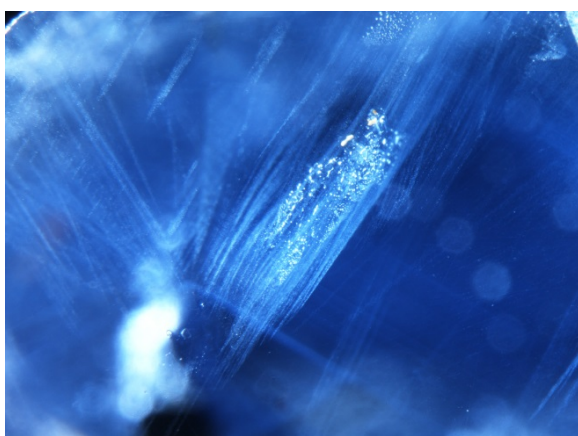
Figure 35: Streamers in GIA sample #9204. Fiber-optic illumination. FOV 2.0 mm. Photo: C. Khowpong © GIA.
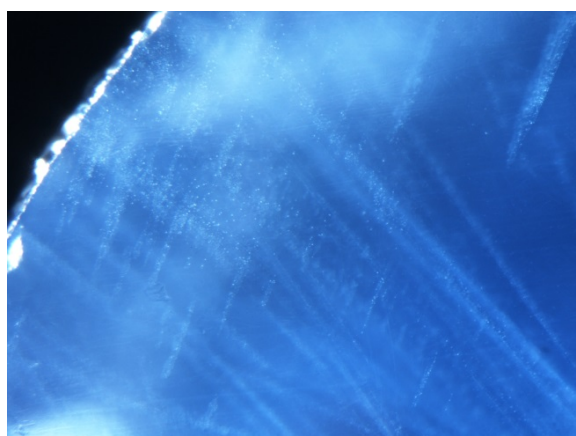
Figure 36: Flake-like inclusion in GIA sample #9204. Fiber-optic illumination. FOV 1.0 mm. Photo: C. Khowpong © GIA.
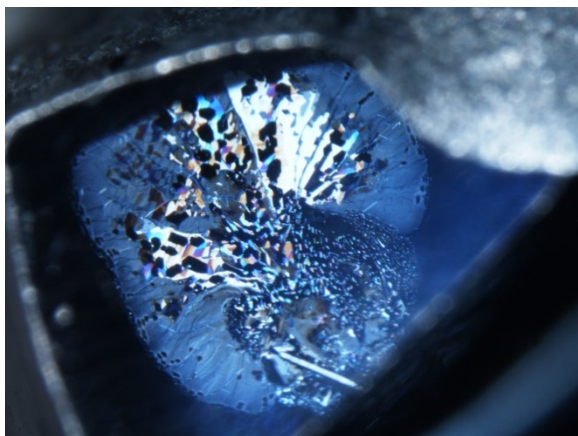
Figure 37: Angular pattern of iridescent partially-healed fissures in GIA sample #2388. Darkfield and fiber-optic illumination. FOV 2.0 mm. Photo: C. Khowpong © GIA.
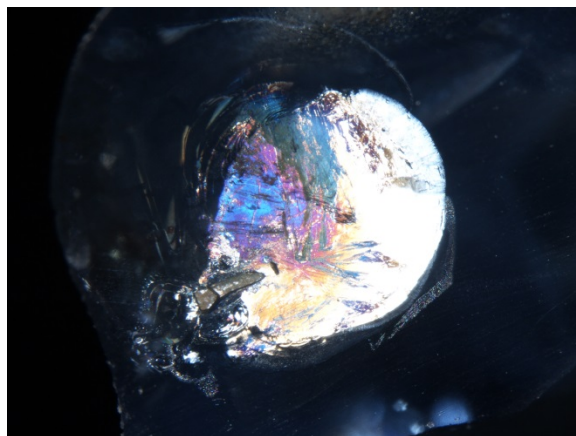
Figure 38: A large decrepitation disc (stress fracture) associated with an unidentified inclusion in GIA sample #9200. Fiber-optic illumination. FOV 2.7 mm. Photo: C. Khowpong © GIA.
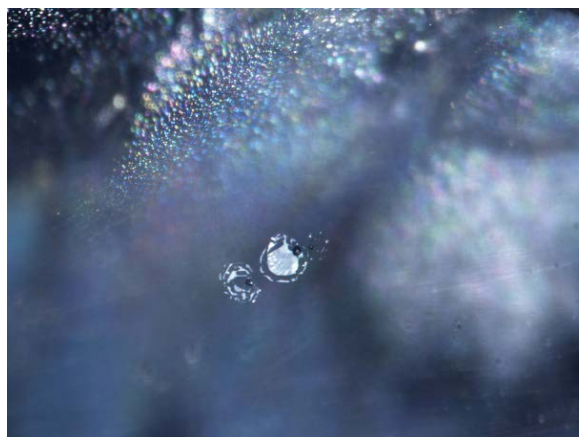
Figure 39: Tiny inclusions associated with naturally-healed fissures in GIA sample #9218. Fiber-optic illumination. FOV 1.07 mm. Photo: C. Khowpong © GIA.
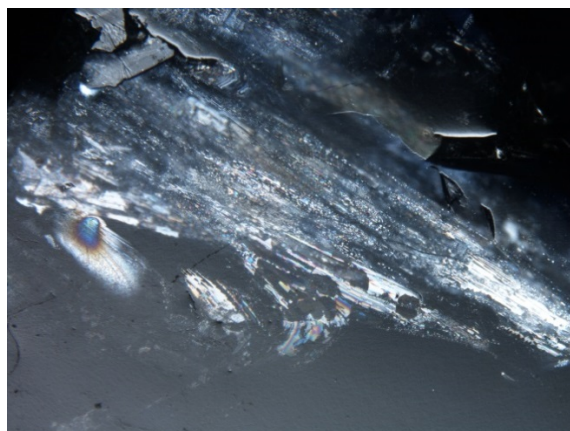
Figure 40: Iridescent thin films in GIA sample #9210. Fiber-optic illumination. FOV 2.7 mm. Photo: C. Khowpong © GIA.

Figure 41: Iridescent natural healed fissure and large reflective fluid inclusions in GIA sample #9210. Fiber-optic illumination. FOV 2.0 mm. Photo: C. Khowpong © GIA.

Figure 42: Unidentified inclusion associated with natural-healed fissures in GIA sample #7132. Darkfield and fiber-optic illumination. FOV 2.0 mm. Photo: J. Muyal © GIA.
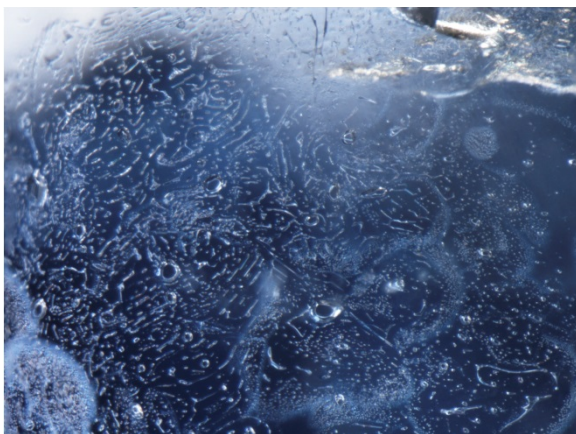
Figure 43: Several unidentified inclusions surrounded fingerprints in GIA sample #7132. Darkfield illumination. FOV 1.5 mm. Photo: J. Muyal © GIA.

Figure 44: Naturally healed fissures with secondary healed fissures in GIA sample #7164. Darkfield illumination. FOV 1.2 mm. Photo: J. Muyal © GIA.

Figure 45: Plane of negative crystals forming a fingerprint in GIA sample #7183. Darkfield and fiber-optic illumination. FOV 1.2 mm. Photo: J. Muyal © GIA.

Figure 46: Naturally-healed fissure with orange stains in GIA sample #1945. Darkfield and diffused illumination. FOV 2.7 mm. Photo: C. Khowpong © GIA.

Figure 47: A scattering of distinct octahedral brownish-red pyrochlore crystals (identified by Raman using the RRUFF database as a reference) in GIA sample #7119. Darkfield and fiber-optic illumination. FOV 1.2 mm. Photo: J. Muyal © GIA.

Figure 48: Pyrochlore crystal (identified by Raman using the RRUFF database as a reference) associated with tension haloes and white tail-like inclusions in GIA sample #7183. Darkfield and fiber-optic illumination. FOV 1.1 mm. Photo: J. Muyal © GIA.

   2017

Figure 49: A brownish red pyrochlore crystal with a 'comet tail' in GIA sample #9203. Fiber-optic illumination. FOV 1.1 mm. Photo: C. Khowpong © GIA.
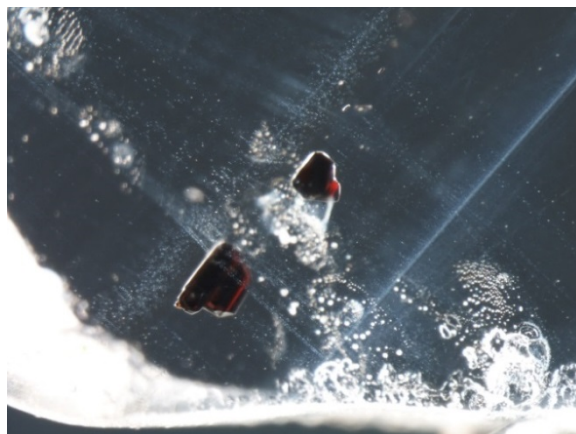
Figure 50: Orthorhombic brownish-red columbite crystals (identified by Raman using the RRUFF database as a reference) in GIA sample #7120. Darkfield illumination. FOV 1.7 mm. Photo: J. Muyal © GIA.
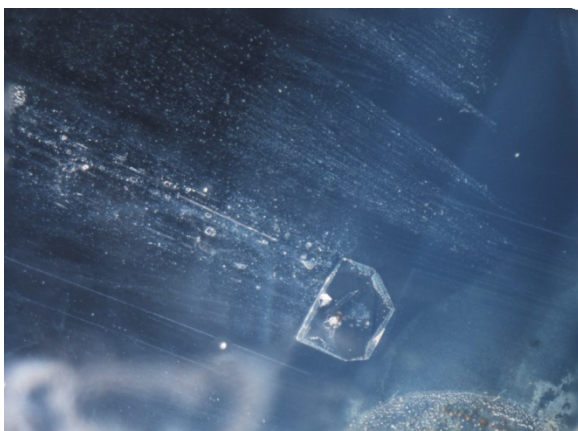
Figure 51: This unidentified doubly reflective crystal acted as a growth obstacle causing comet tail-like streamers in GIA reference #7183. Darkfield and fiber-optic illumination. FOV 1.1 mm. Photo: J. Muyal © GIA.
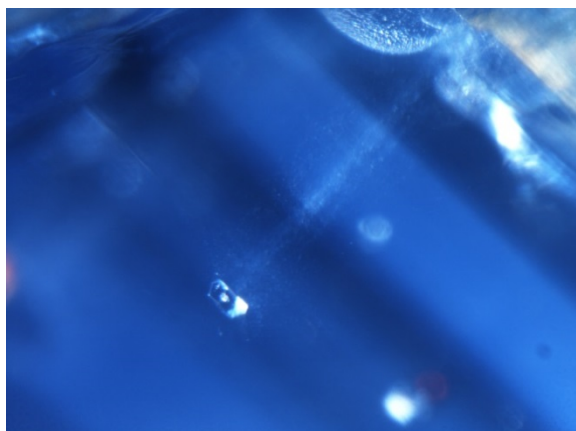
Figure 52: A colorless unidentified crystal with a 'comet tail' in GIA sample #9203. Darkfield and fiber-optic illumination. FOV 1.1 mm. Photo: C. Khowpong © GIA.

Figure 53: Black unidentified opaque inclusion with decrepitation disk in GIA sample #1945. Fiber-optic illumination. FOV 1.3 mm. Photo: C. Khowpong © GIA.
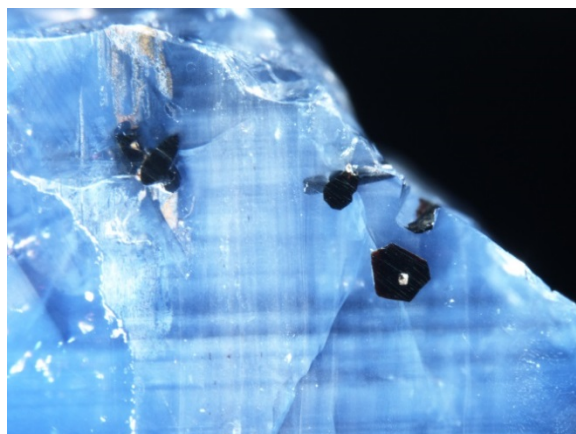
Figure 54: Black unidentified opaque inclusions with decrepitation disks in GIA sample #1975. Fiber-optic illumination. FOV 2.7 mm. Photo: C. Khowpong © GIA.
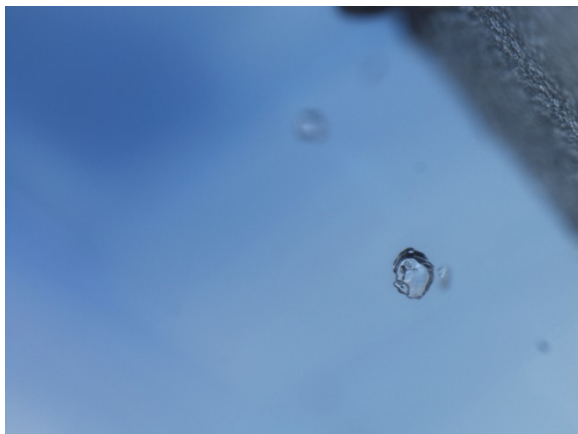
Figure 55: Feldspar is frequently found in basalt-related blue sapphires (identified by Raman using the RRUFF database as a reference). This example is in GIA sample #2389. Darkfield and diffused illumination. FOV 1.3 mm. Photo: J. Muyal © GIA.

Figure 56: Well-formed feldspar crystal (identified by Raman using the RRUFF database as a reference) in GIA sample #2389. Darkfield and diffused illumination. FOV 1.5 mm. Photo: J. Muyal © GIA.

Figure 57: Feldspar crystal with rounded appearance (identified by Raman using the RRUFF database as a reference) in GIA sample #7132. Darkfield illumination. FOV 1.1 mm. Photo: J. Muyal © GIA.

Figure 58: Three unidentified crystals in GIA sample #8502. Darkfield and fiber-optic illumination. FOV 1.1 mm. Photo: J. Muyal © GIA.
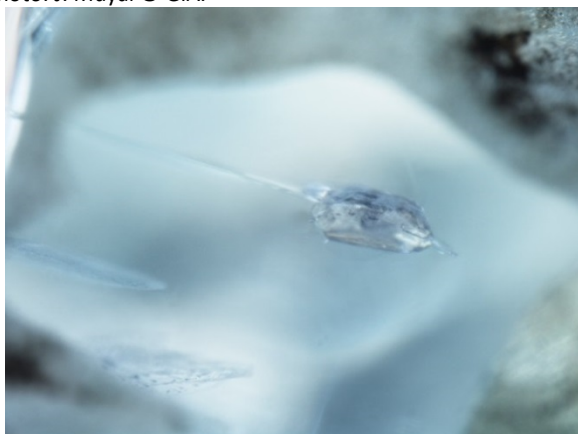
Figure 59: Zircon crystal (identified by Raman using the RRUFF database as a reference) in GIA sample #7132. Darkfield illumination. FOV 1.7 mm. Photo: J. Muyal © GIA.

Figure 60: A prismatic zircon crystal (identified by Raman using the RRUFF database as a reference) in GIA sample #9197. Darkfield and fiber-optic illumination. FOV 1.3 mm. Photo: C. Khowpong © GIA.
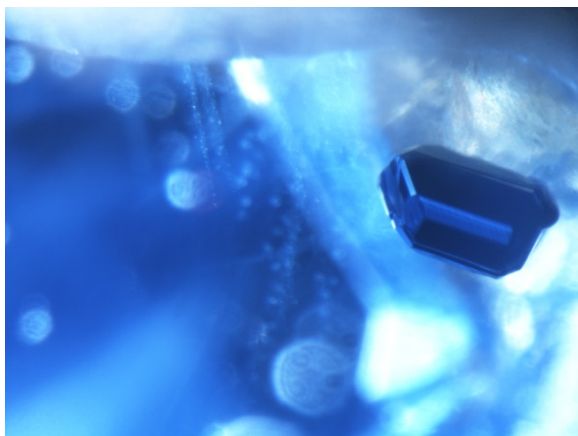
Figure 61: Orthorhombic columbite crystal in GIA sample #9204. Darkfield and fiber-optic illumination. FOV 1.1 mm. C. Khowpong © GIA.
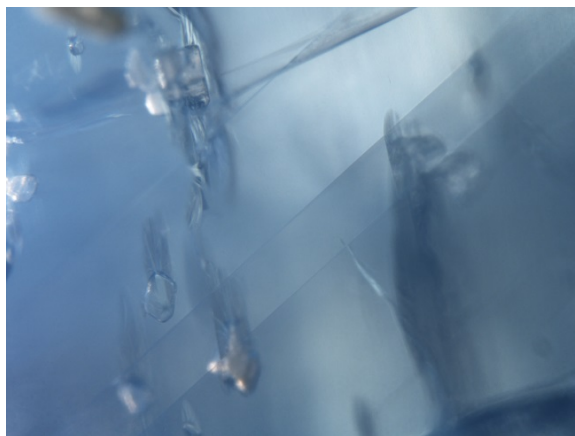
Figure 62: Feldspar inclusions in GIA sample #1942. Darkfield and fiber-optic illumination. FOV 1.6 mm. C. Khowpong © GIA.

Figure 63: Trapiche pattern and hexagonal zoning in GIA sample #1981. Darkfield and fiber-optic illumination. FOV 4.0 mm. Photo: C. Khowpong © GIA.

Figure 64: Trapiche pattern and thin films in GIA sample #1981. Fiber-optic illumination. FOV 4.0 mm. Photo: C. Khowpong © GIA.

3.2 Spectroscopy and chemistry of blue sapphires from Pailin, Cambodia

3.2.1 UV-VIS-NIR SPECTROSCOPY

UV-Vis-NIR spectra of Pailin sapphires show typical features of basalt-related blue sapphire including Fe^{3+} and Fe^{2+}-Ti^{4+} pairs along with a broad band around 840-800 nm in the near-infrared region. The possible absorption features that might be present in blue sapphire are (Ferguson, 1971, 1972; Hughes, 2017; chapter 4):

- An absorption shoulder at about 330 nm assigned to Fe^{3+}- Fe^{3+} pairs. Its absorption strength increases more rapidly than the single Fe^{3+} ions.
- A peak at 377 and 450 nm assigned to Fe^{3+}- Fe^{3+} pairs. These absorption peaks are distinctly and clearly due to high Fe content.
- A peak at 388 nm assigned to single Fe^{3+} ions, therefore the absorption coefficient will increase linearly with Fe^{3+} concentration.
- A broad absorption band at 580 nm assigned to Fe^{2+}- Ti^{4+} pairs, giving a blue color.
- A broad absorption band around 840-880 nm at near infrared region which is characteristic of natural basalt-related blue sapphires. It is often attributed to Fe^{2+}- Fe^{3+} pairs (Smith, 1977, 1978; Smith & Strens, 1976). Note that Fe^{2+} in corundum is an acceptor; therefore it requires charge compensation by electron donors such as Si^{4+}or Ti^{4+}. This broad band is not clearly understood and requires further study. It could be due to charge compensation between Fe^{2+} and Ti^{4+}, Si^{4+} or both, as described in Hughes, 2017, chapter 4.

Two samples, (GIA #8602 and #2389) were selected to provide representative UV-Vis-NIR spectra for Pailin sapphire, (see below). FTIR and chemistry were collected in the same area.

Blue Sapphire from GIA sample #8602
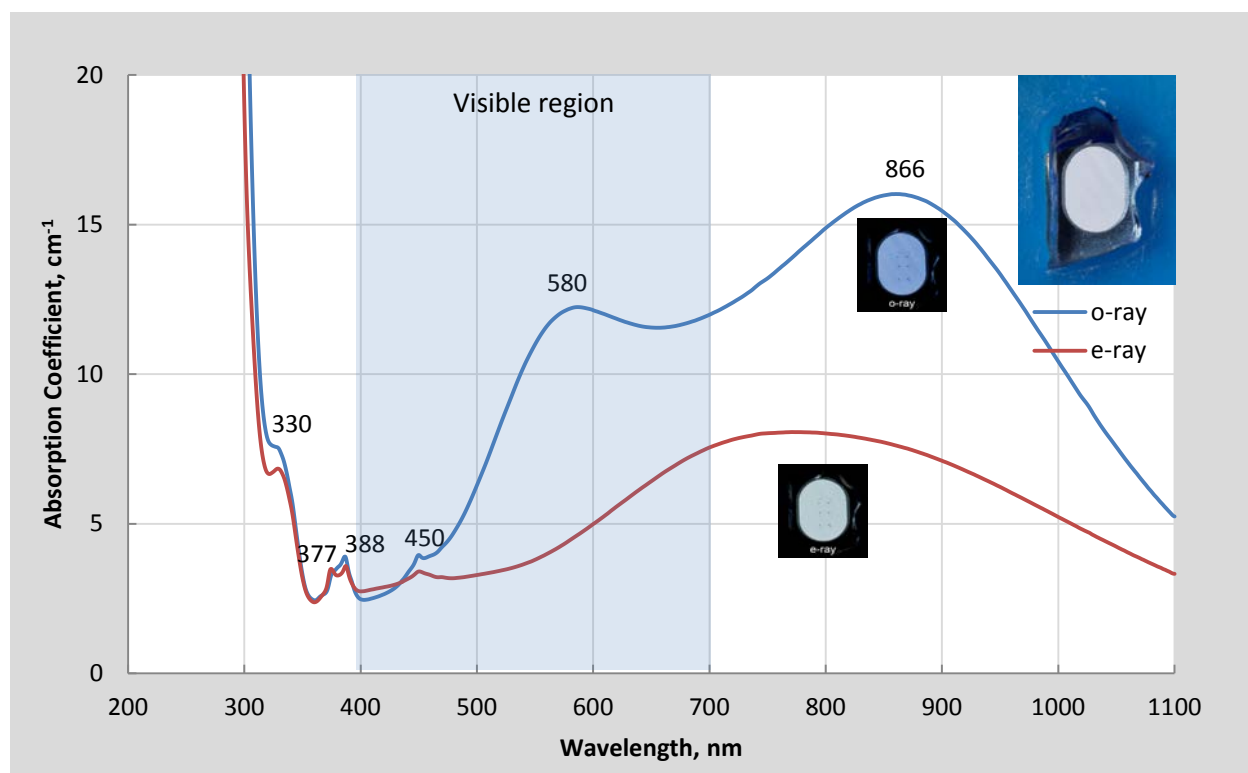
Figure 65: UV-Vis-NIR absorption spectra of GIA reference sample #8602 with inset color calibrated polarized photos of the beam path area for the o- and e-rays. Optical path length: 1.036 mm. Alpha max=35 cm^{-1}.

The obtained UV-Vis-NIR spectra for sample #8602 (figure 65) presented a broad absorption band for the o-ray starting around 450 nm and increasing towards the red part of the visible spectrum. This feature is related to intervalence charge transfer absorption by Fe^{2+}-Ti^{4+} pairs. The blue color is produced by an average of 32 ppma of titanium content associated with iron. A spectral feature or shoulder at 330 nm is also present due to medium iron content. The main absorption feature in the o-ray's NIR spectrum of is a strong band between 840-900 nm. In contrast, the e-ray shows absorption between 730-820 nm, which is seen in all natural basalt-related sapphire. This feature absorbs outside the visible part of the spectrum and is thus not responsible for the blue color seen by human eyes.

The chemical data collected (figure 66, table 2) showed a very limited amount of trace elements. Only significant amounts of iron (Fe), gallium (Ga), and titanium (Ti) were detected. Magnesium (Mg) and chromium (Cr) were below the detection limit. A small amount of vanadium (V) was found. The iron content showed in the medium range of 909 ppma. Ti content ranges from 27-36 ppma, giving a medium blue color. Traces of tantalum (Ta) were detected, but Be, Nb, Sn, Zr, Hf, W, and Th were absent.
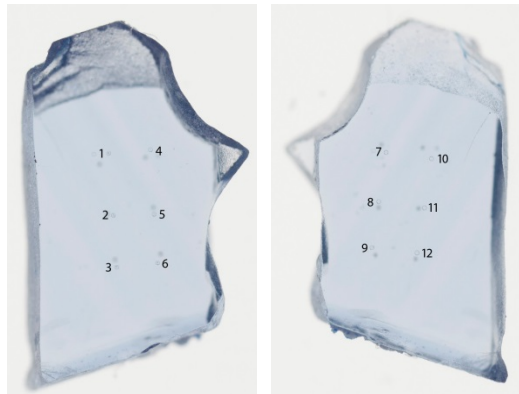
Color calibrated using transmitted illumination   *Bright field and diffused illumination*

Figure 66: GIA sample #8602 showing the location of the 12 spots where LA-ICP-MS analysis was conducted on each side of the wafer. Left: Color calibrated and transmitted illumination. Field of view 6.0 mm. Photo: S. Engniwat © GIA. Right: Brightfield and diffused illumination. Field of view 2.0 mm. Photo: U. Atikarnsakul © GIA.

Table 2: LA-ICP-MS results in parts per million atomic (ppma) units for GIA sample #8602. "BDL" stands for "Below Detection Limit", "BQL" stands for "Below Quantification Limit"

| GIA sample #8602 Spot number (color of the area)	^{9}Be	^{24}Mg	^{47}Ti	^{51}V	^{52}Cr	^{57}Fe	^{69}Ga	^{90}Zr	^{93}Nb	^{120}Sn	^{178}Hf	^{181}Ta	^{182}W	^{232}Th
SP1 (medium blue)	BDL	BDL	36	3	BDL	960	47	0.12	BDL	BDL	BDL	0.01	BDL	BDL
SP2 (medium blue)	BDL	BDL	30	3	BDL	953	48	0.00	0.02	BDL	BDL	0.12	BDL	BDL
SP3 (medium blue)	BDL	BDL	31	3	BDL	971	47	0.02	BQL	BDL	BDL	0.01	BDL	BDL
SP4 (medium blue)	BDL	BDL	31	3	BDL	924	47	0.13	BDL	BDL	BDL	0.01	BDL	BDL
SP5 (medium blue)	BDL	BDL	34	3	BDL	920	47	0.04	0.00	BDL	BDL	0.01	BDL	BDL
SP6 (medium blue)	BDL	BDL	27	3	BDL	957	46	0.06	BQL	BDL	BDL	0.01	BDL	BDL
SP7 (medium blue)	BDL	BDL	28	3	BDL	836	42	BDL	BQL	BDL	BQL	0.01	0.00	BDL
SP8 (medium blue)	BQL	BDL	35	3	BDL	869	46	BDL	BQL	BDL	0.00	0.02	BDL	BDL
SP9 (medium blue)	BDL	BDL	29	3	BDL	935	46	BDL	0.01	BDL	BQL	0.02	BDL	BDL
SP10 (medium blue)	BDL	BDL	28	3	BDL	840	43	BDL	BDL	BDL	BDL	0.01	BDL	BDL
SP11 (medium blue)	BDL	BDL	31	3	BDL	862	44	0.00	0.03	BDL	BDL	0.16	BDL	BQL
SP12 (medium blue)	BDL	BDL	35	3	BDL	887	45	BDL	0.01	BDL	BDL	0.06	BDL	BDL
Average±SD	-	-	**31±3**	**3±0.2**	-	**909±49**	**46±2**	-	-	-	-	**0.04±0.05**	-	-
Detection limit	0.3	0.04	0.5	0.1	1.0	5.9	0.02	0.0004	0.001	0.05	0.0002	0.0001	0.0008	0.0001

Blue Sapphire from GIA sample #2389

Figure 67: UV-Vis-NIR absorption spectra of GIA reference specimen #2389 with inset color calibrated polarized photos of the beam path area for the o- and e-rays. Optical path length: 2.80 mm. Alpha max=11.7cm^{-1}.

Color calibrated using transmitted illumination
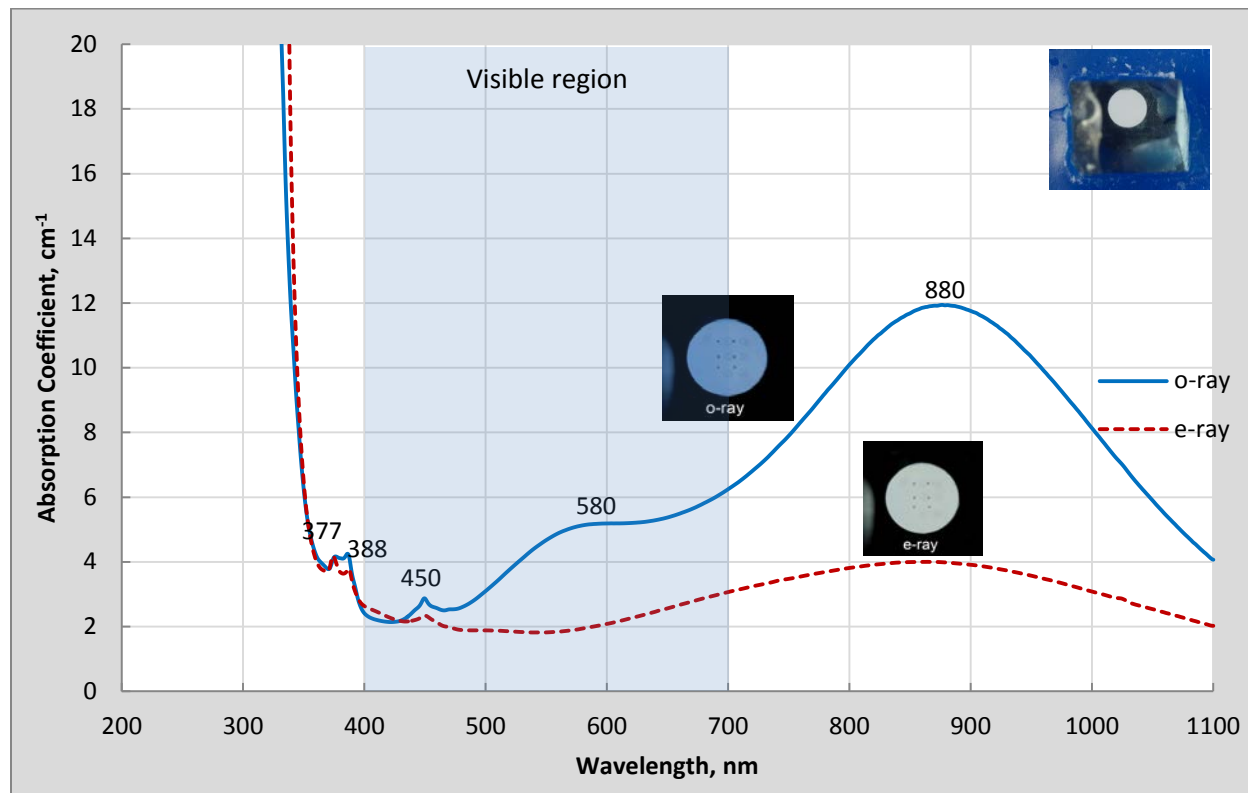
Fiber-optic illumination

Figure 68: GIA sample #2389 showing the location of the 12 spots where LA-ICP-MS analysis was conducted on each side of the wafer. Left: Color calibrated and transmitted illumination. Field of view 6.00 mm. Photo: S. Engniwat © GIA. Right: Fiber optic illumination. Field of view 8.2 mm. Photo: U. Atikarnsakul © GIA.
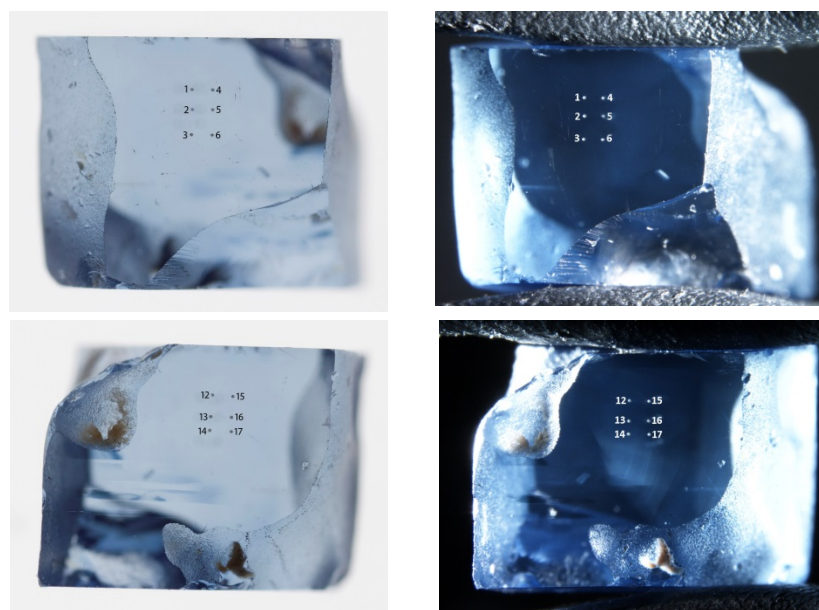
Table 3: LA-ICP-MS results in parts per million atomic (ppma) units for GIA sample #2389. "BDL" stands for "Below Detection Limit", "BQL" stands for "Below Quantification Limit"

GIA sample #2389 Spot number (color of the area)	^{9}Be	^{24}Mg	^{47}Ti	^{51}V	^{52}Cr	^{57}Fe	^{69}Ga	^{90}Zr	^{93}Nb	^{120}Sn	^{178}Hf	^{181}Ta	^{182}W	^{232}Th
SP1 (blue, weak cloud)	BQL	BQL	155	11	BDL	876	82	BQL	0.03	0.26	0.00	0.18	BDL	BDL
SP2 (blue, weak cloud)	2	BQL	128	11	BDL	891	83	0.01	0.78	0.34	0.01	2.51	BDL	0.00
SP3 (blue, weak cloud)	0.5	BDL	124	11	BDL	865	82	BDL	0.04	0.20	BDL	0.15	BQL	BDL
SP4 (blue, weak cloud)	0.8	1.2	147	10	BDL	891	82	0.01	0.05	0.30	0.00	0.21	BDL	BDL
SP5 (blue, weak cloud)	4	BQL	129	10	BDL	869	83	0.01	1.11	0.29	BDL	3.69	BQL	0.01
SP6 (blue, weak cloud)	BQL	BQL	106	11	BDL	865	82	BQL	0.04	0.18	BDL	0.12	BDL	BDL
SP7 (blue, weak cloud)	0.3	0.9	229	13	6	927	81	0.01	0.05	0.44	0.00	0.14	BDL	BDL
SP8 (blue, weak cloud)	0.6	0.9	224	12	6	913	81	BDL	0.05	0.55	0.00	0.14	BDL	BDL
SP9 (blue, weak cloud)	5	1.0	226	12	5	935	80	0.01	1.89	0.58	0.01	4.17	0.01	0.01
SP10 (blue, weak cloud)	0.6	1.2	221	12	5	924	80	BQL	0.05	0.42	0.00	0.17	BDL	BDL
SP11 (blue, weak cloud)	0.3	1.1	199	12	6	898	79	0.00	0.06	0.38	0.00	0.17	BDL	0.00
SP12 (blue, weak cloud)	0.6	0.9	221	12	5	909	78	0.01	0.04	0.52	0.00	0.17	BDL	BDL
Average±SD	-	-	175±48	11±0.8	-	896±24	80.9±1.7	-	0.35±0.60	0.37±0.13	-	0.99±1.53	-	-
Detection limit	0.2	0.4	0.7	0.1	0.5	3.4	0.02	0.002	0.002	0.04	0.0008	0.0002	0.001	0.000

UV-Vis-NIR spectra for sample #2389 (figure 67) displayed absorption features of both single Fe^{3+} and Fe^{2+}-Ti^{4+} pairs along with a broad band at about 880 nm as described above. Due to cloud inclusions, there was no shoulder observed about 330 nm, as small particles may scatter the light and thus less light reaches to the detector. This does not mean that light is absorbed although it gives the same signal for this device. Scattering is more effective at shorter wavelengths thus we might observe an increased absorption edge at lower wavelengths when measured in particles or cloud. An average of the available Ti, (175 ppma), would typically be expected to create a very dark blue or black and give strong absorption at 580 nm. However, this wasn't the case with sample #2389. The high Ti content detected in GIA sample #2389 might be from minute rutile inclusions.

The collected chemical data (figure 68, table 3) showed a very limited amount of trace elements. Only significant amounts of iron (Fe), gallium (Ga), and titanium (Ti) were detected. Magnesium (Mg) and chromium (Cr) were below the instrument's detection limit. Small amounts of vanadium (V) were found. The iron content showed in the medium range (896 ppma on average). Ti—which is related to exsolved rutile particles—was found in the range of 106 to 229 ppma, together with other elements such as Be, Nb, Sn, and Ta.

3.2.2 FOURIER TRANSFORM INFRARED SPECTROSCOPY OR FTIR

We characterized sixty (60) samples from Pailin, Cambodia. Most samples exhibited 3309 series bands (3232 and 3186 cm^{-1}) which are indicative of natural basalt-related blue sapphire (Smith 1995; Beran 2006). Kaolinite was commonly detected in Pailin sapphire. We characterized the observed FTIR features as follows (figure 69):

    i) 33 samples with 3309 series absorption features (3232, and 3186 cm^{-1} or 3295, 3232, 3186 cm^{-1}) and sometimes with peaks at 3367, 3378, 3394 cm^{-1}, (figure 67a, b)

    ii) 8 samples where the absorption peak at 3232 cm^{-1} is stronger than the 3309 cm^{-1} peak (figure 67c)

    iii) 2 samples which only displayed an absorption feature of 3309 cm^{-1}

We identified the intensity of peak height on 18 samples. Results showed the peak at 3309 cm^{-1} ranged from 0.16 to 6.73 cm^{-1} and the peak at 3232 cm^{-1} from 0.007 cm^{-1} up to 1.591 cm^{-1}. Three (3 out of 18) samples had a peak of 3232 cm^{-1} higher than 3309 cm^{-1}, see Table 4.
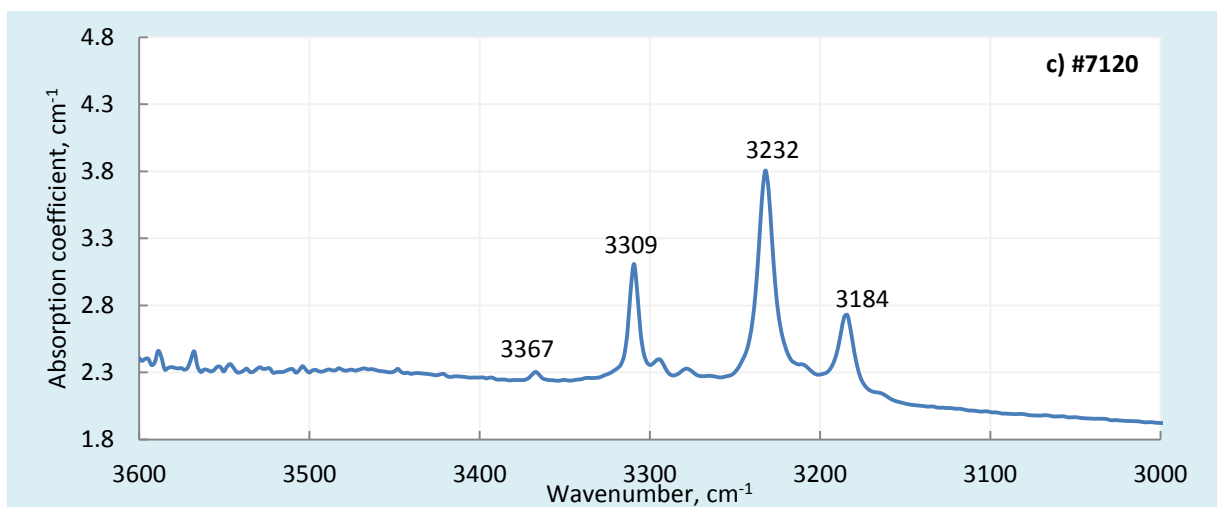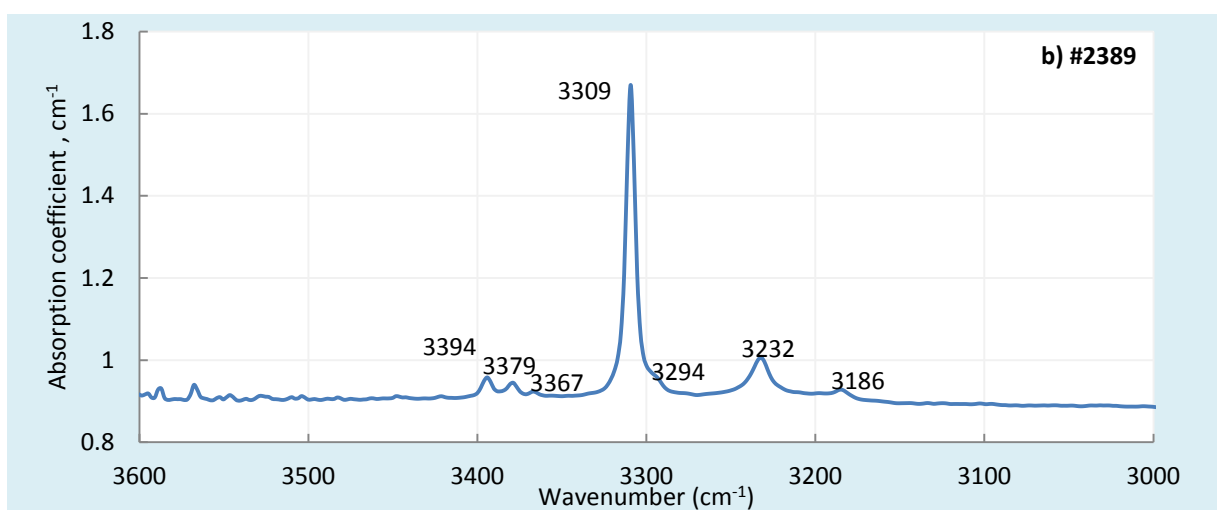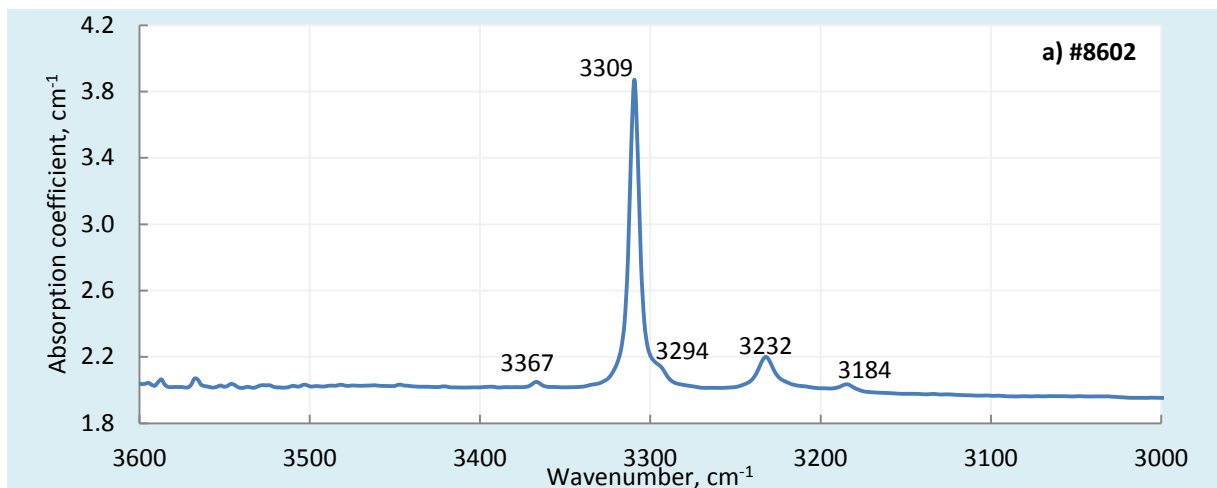
Figure 69: FTIR spectrum of GIA reference specimen #8602, #2389, and #7120 in the 2800 to 3600 cm^{-1} range.
Optical path length: a) 1.036; b) 2.796, and c) 0.58 mm. * Due to the lack of a polarizer couldn't obtain accurate polarized light FTIR spectra.

Table 4: FTIR peaks observed in the 18 sapphire samples from Pailin region, Cambodia

GIA sample	Wafer window orientation	Relative peak intensity (peak height, cm⁻¹)				
		3367 cm⁻¹ series	3309cm⁻¹	3232 cm⁻¹	3186 cm⁻¹	Mineral peak
#8502	⊥* to c-axis	very weak (0.036)	**Strongest (1.637)**	Weak (0.100)	very weak (0.017)	-
#8602	Un-oriented**	very weak (0.052)	**Strongest (1.862)**	Weak (1.175))	very weak (0.033)	-
#8102	⊥ to c-axis	-	**Strongest (1.320)**	Weak (0.790)	very weak (0.012)	-
#8202	⊥ to c-axis	-	**Strongest (0.221)**	Weak (0.009)	-	-
#2384	Un-oriented	very weak (0.001)	**Strongest (0.128)**	Weak (0.008)	-	-
#2388	Un-oriented	very weak (0.014)	**Strongest (0.633)**	Weak (0.035)	very weak (0.008)	-
#2389	⊥ to c-axis	very weak (0.047)	**Strongest (0.757)**	Weak (0.095)	very weak (0.024)	-
#2390	Un-oriented	very weak (0.012)	**Strongest (1.012)**	Weak (0.079)	very weak (0.012)	-
#5043	Un-oriented	-	**Strongest (0.161)**	Weak (0.007)	-	-
#7119	Un-oriented	very weak (0.104)	Medium (1.535)	**Strongest (1.899)**	Weak (0.735)	-
#7120	⊥ to c-axis	very weak (0.059)	Medium (0.856)	**Strongest (1.591)**	Weak (0.601)	-
#7122	⊥ to c-axis	-	**Strongest (0.762)**	Weak (0.042)	-	-
#7129	⊥ to c-axis	-	Weak (0.016)	-	-	kaolinite
#7132	⊥ to c-axis	-	**Strongest (2.232)**	Weak (0.102)	-	-
#7133	Un-oriented	-	**Strongest (6.733)**	Weak (0.263)	-	kaolinite
#7164	Un-oriented	very weak (0.005)	**Strongest (0.391)**	Weak (0.024)	very weak (0.004)	-
#7172	⊥ to c-axis	very weak (0.104)	**Strongest (4.404)**	Weak (0.971)	very weak (0.262)	-
#7183	⊥ to c-axis	very weak (0.105)	Medium (1.855)	**Strongest (2.068)**	Weak (0.809)	-

* Optical wafer is perpendicular to c-axis, ** Un-oriented is either from un-oriented samples or optical wafer parallel to c-axis.
Due to, without a polarizer couldn't obtain accurate polarized light FTIR spectra.

3.2.3 CHEMICAL ANALYSIS

Chemical analysis of Pailin sapphires provided similar results to other basalt-related blue sapphires. We found Mg in amounts ranging from insignificant up to 12 ppma. Ti showed a wide range, which is dependent on the density of clouds and particles, ranging from 3 to 404 ppma in areas with fewer clouds, or from 28 to 579 ppma in areas with dense clouds or particles. We found Fe in concentrations up to 2005 ppma and 3761 ppma in areas with less and areas with dense clouds or particles respectively. We detected V in amounts up to 22 ppma. We only detected Cr in two samples in concentrations between 2 and 13 ppma. Owning to the fact that most of the Pailin sapphire samples contained milky clouds, natural Be—along with Nb and Ta—was commonly detected, (see table 9). We selected the following samples to represent chemistry in this report:

Blue Sapphire of GIA sample #8102

GIA sample #8102 contained strong internal growth features which related to milky fine grained clouds. Under diffused illumination, blue and brown color zoning were observed, which were related to areas with milky clouds (figure 70). We then analyzed chemistry on these two areas, see table 5 .

Sp 6-10   Sp 11-15
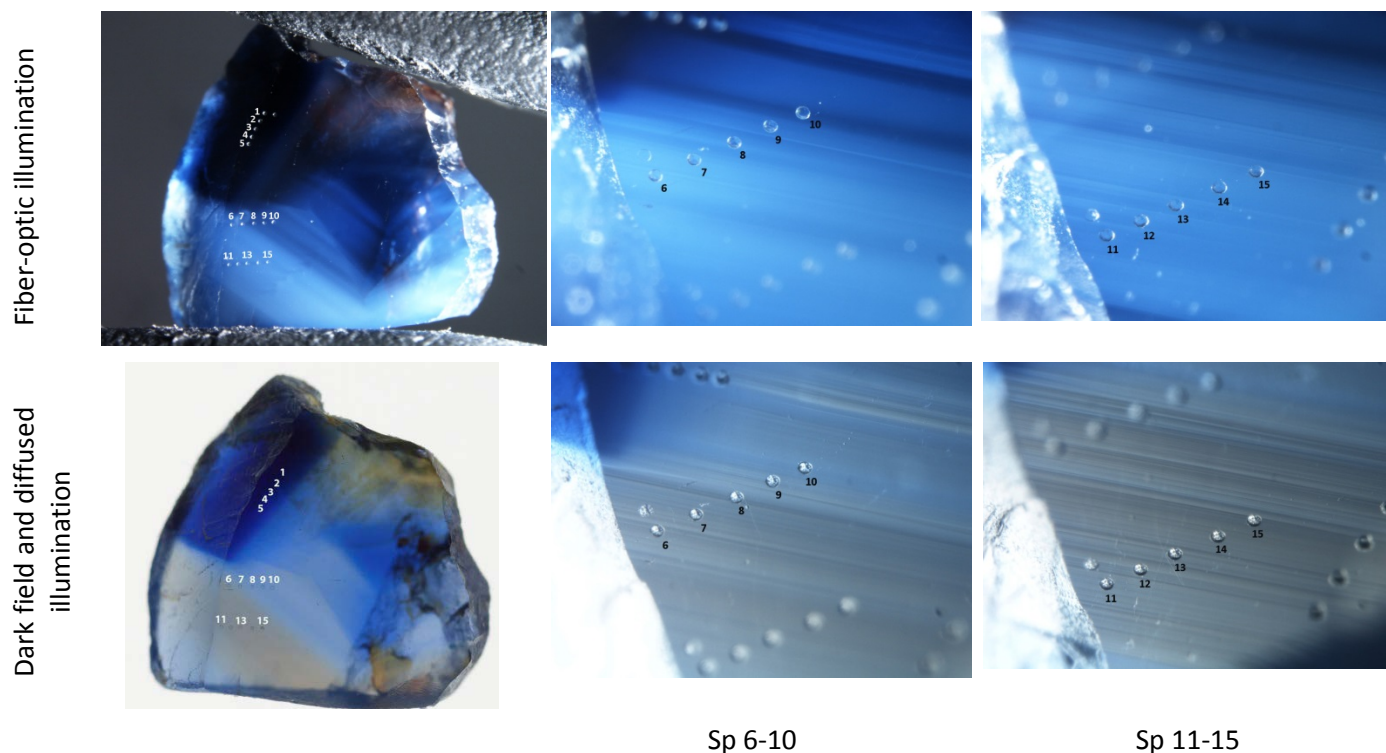
Figure 70: GIA sample #8102 showing the location of the 15 spots where LA-ICP-MS analysis was conducted on the different areas. The photos were captured using fiber optic illumination (top) and darkfield and diffused illuminations (bottom). Photo: U. Atikarnsakul © GIA.

Table 5: LA-ICP-MS results in parts per million atomic (ppma) units for GIA sample #8102.

| GIA sample #8102 Spot number (color of the area)	[9]Be	[24]Mg	[47]Ti	[51]V	[52]Cr	[56]Fe	[69]Ga	[90]Zr	[93]Nb	[120]Sn	[178]Hf	[181]Ta	[182]W	[232]Th
sp1 (blue zoning)	3	9	430	10	BDL	1596	66	0.03	10.12	0.52	0.00	7.29	BDL	0.03
sp2 (blue zoning)	5	10	434	9	BDL	1680	55	0.04	10.25	0.62	BQL	7.08	BQL	0.05
sp3 (blue zoning)	4	9	443	10	BDL	1621	53	0.04	10.34	0.58	BQL	7.48	BDL	0.03
sp4 (blue zoning)	4	9	430	10	BDL	1541	54	0.03	10.16	0.59	0.00	7.11	BQL	0.03
sp5 (blue zoning)	3	9	422	10	BDL	1570	55	0.04	8.58	0.50	0.00	7.26	BDL	0.02
sp6 (dense milky cloud)	2	3	411	8	BDL	1227	50	0.07	1.35	0.60	0.01	1.78	BQL	0.007
sp7 (dense milky cloud)	1.3	3	439	8	BDL	1303	49	0.09	1.99	0.69	0.01	2.48	BQL	0.015
sp8 (milky cloud)	BQL	1	148	6	BDL	1245	47	0.00	0.03	0.19	BDL	0.10	BDL	BDL
sp9 (milky cloud)	0.9	2	191	5	BDL	1267	46	0.02	0.25	0.40	0.01	0.59	BDL	0.001
sp10 (milky cloud)	BQL	BQL	78	4	BDL	1387	43	0.00	0.02	0.16	0.00	0.07	BDL	BQL
sp11 (dense milky cloud)	BDL	3	321	7	BDL	1424	48	0.03	0.51	0.44	0.00	0.82	BQL	0.003
sp12 (dense milky cloud)	2	3	317	7	BDL	1424	54	0.03	0.63	0.52	0.01	0.92	BDL	0.004
sp13 (dense milky cloud)	BQL	3	342	7	BDL	1435	49	0.03	0.45	0.50	BDL	0.79	BDL	0.003
sp14 (dense milky cloud)	2	3	421	8	BDL	1574	49	0.05	0.77	0.56	0.01	1.25	BDL	0.004
sp15 (dense milky cloud)	2	3	400	7	BDL	1344	51	0.04	0.58	0.53	0.01	0.99	BDL	0.001
Average±SD	-	-	349±118	8±2	-	1442±147	51±6	0.04±0.02	3.7±4.5	0.5±0.1	-	3.1±3.1	-	-
Detection limit	0.1	0.2	0.8	0.1	0.3	0.8	0.03	0.003	0.003	0.04	0.001	0.001	0.002	0.001

Sample #8102 showed minor elements such as iron (Fe), gallium (Ga), and titanium (Ti) that are commonly detected in basalt-related blue sapphire. Small amounts of magnesium (Mg) and vanadium (V) were present, but Cr was absent. We found Fe in higher levels up to an average of 1442 ppma. Two areas—blue color zoning and clouds—presented slightly different chemistries. Blue color zoning showed higher amounts of beryllium (Be)—which correlate with titanium (Ti), niobium (Nb), tantalum (Ta), and thorium (Th)—than in dense milky clouds. The amounts of Nb, Ta, and Th in the blue color zoning are much higher than in areas with dense milky clouds. Ti content is insignificant or found up to 443 ppma in blue color zoning and 439 ppma in dense milky clouds. The correlations between laser spots and trace elements in different areas showed a very good correlation between Be, Mg, Ti, Nb, Sn and Ta (Figure 71).
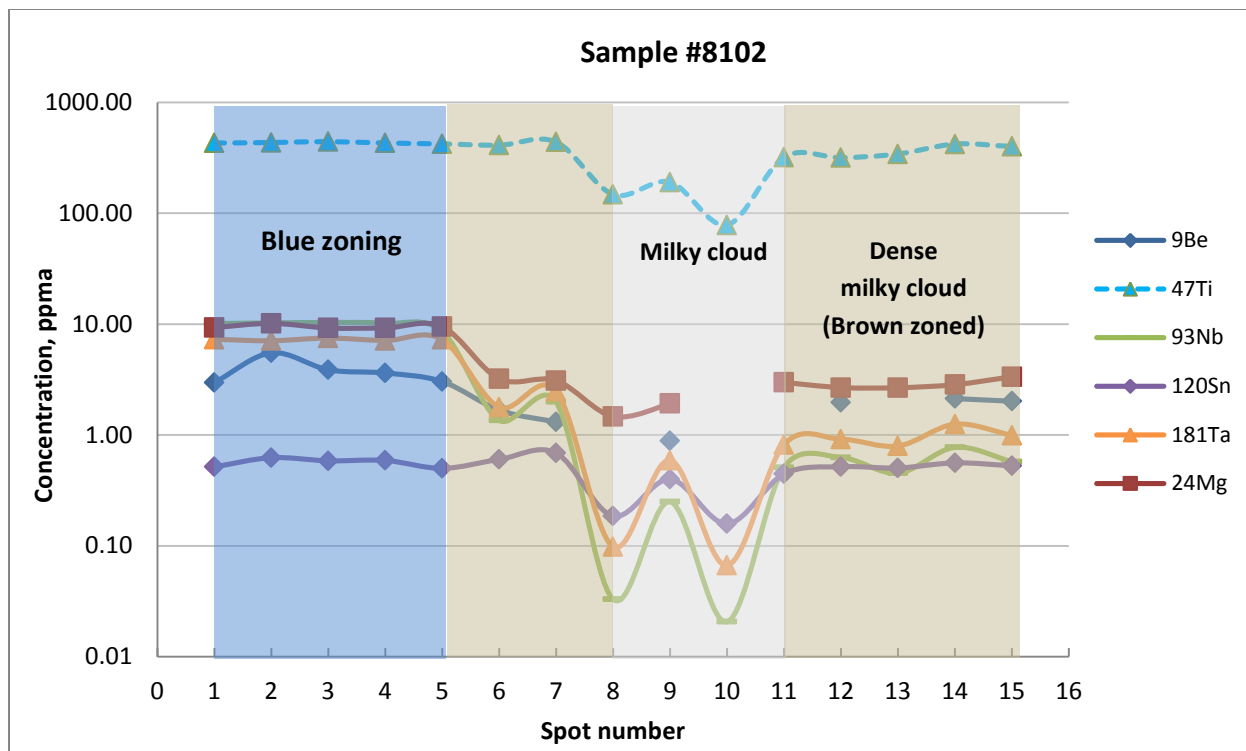
Figure 71: Correlation between laser spots and trace elements in different particle areas on GIA sample #8102 indicating natural Be in sapphire.

Blue Sapphire from GIA sample #9206

GIA sample #9206 contained very strong blue zoning, internal growth, milky clouds, stringers, comet tails, intersecting growth tubes, high-relief crystal with healed fractures. One area of near-colorless zoning had very weak fine milky clouds. We analyzed chemistry in different areas as shown below (figure 72).
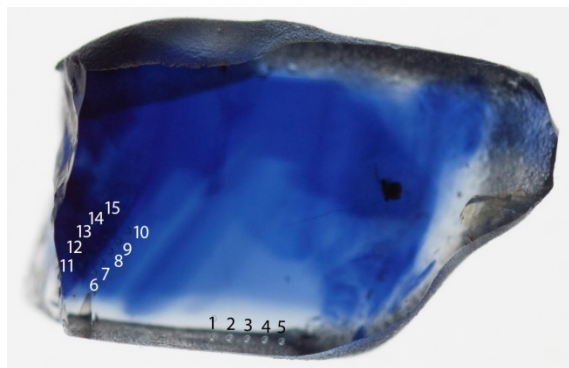
Figure 72: GIA sample #9206 showing the location of the 15 spots where LA-ICP-MS analysis was conducted on different areas. Top: Color calibrated with transmitted illumination. Photo: S. Engniwat © GIA. Bottom: Bright-field and fiber optic illumination**.** Photo: U. Atikarnsakul © GIA.

Table 6: LA-ICP-MS results in parts per million atomic (ppma) units for GIA sample #9206.

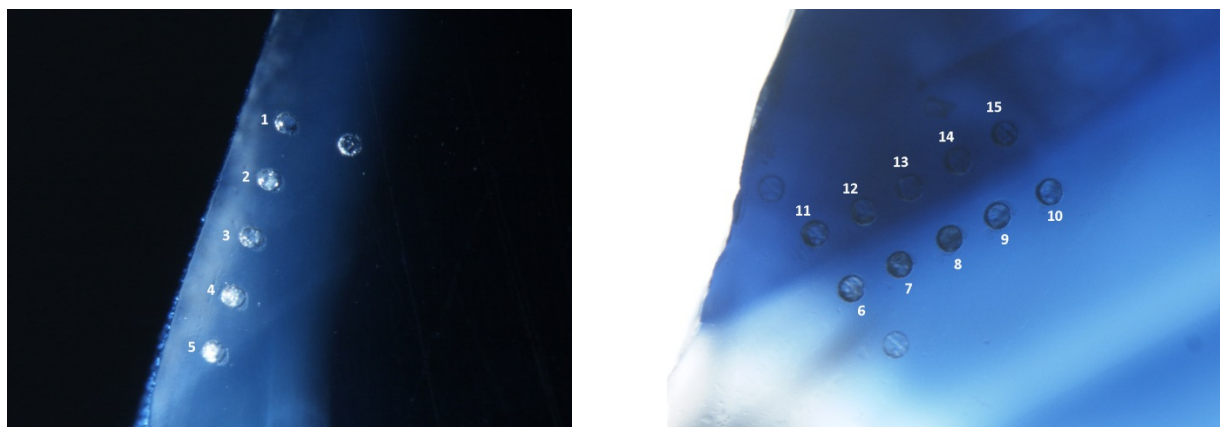| GIA sample #9206 Spot number (color of the area)	^{9}Be	^{24}Mg	^{47}Ti	^{51}V	^{52}Cr	^{56}Fe	^{69}Ga	^{90}Zr	^{93}Nb	^{120}Sn	^{178}Hf	^{181}Ta	^{182}W	^{232}Th
sp1 (milky cloud)	20	5	155	20	BDL	1891	89	0.12	23	4.96	0.03	30	0.003	0.25
sp2 (milky cloud)	15	5	122	20	BDL	1877	87	0.11	14	4.07	0.03	26	0.005	0.18
sp3 (milky cloud)	12	4	119	19	BDL	1931	89	0.09	13	3.97	0.02	24	BDL	0.18
sp4 (milky cloud)	15	5	126	21	BDL	1953	91	0.10	13	4.09	0.02	25	0.000	0.17
sp5 (milky cloud)	14	5	120	20	BDL	1899	90	0.09	12	4.00	0.03	24	0.002	0.16
sp6 (milky cloud)	27	6	272	20	BDL	2030	100	0.23	40	6.18	0.04	40	0.007	0.33
sp7 (milky cloud)	24	6	270	19	BDL	1913	97	0.17	36	6.03	0.03	38	0.010	0.31
sp8 (milky cloud)	27	6	276	21	BDL	1928	96	0.22	37	6.12	0.03	38	0.008	0.31
sp9 (milky cloud)	30	6	279	20	BDL	2245	100	0.17	38	6.22	0.03	39	0.005	0.30
sp10 (milky cloud)	24	6	268	20	BDL	1968	101	0.18	34	5.86	0.03	38	0.004	0.27
sp11 (blue zoning)	7	7	410	21	BDL	2125	97	0.01	8	1.69	0.00	8	0.002	0.02
sp12 (blue zoning)	10	8	447	22	BDL	2081	102	0.07	19	2.63	0.01	13	0.003	0.11
sp13 (blue zoning)	6	7	443	22	BDL	2037	102	0.02	11	1.91	0.00	8	0.003	0.04
sp14 (blue zoning)	4	7	451	22	BDL	2107	104	0.03	14	1.98	0.01	10	0.003	0.07
sp15 (blue zoning)	6	6	464	22	BDL	2067	101	0.02	11	1.96	0.00	8	0.004	0.04
Average±SD	16±8	6±1	282±133	21±1	-	2004±106	96±6	0.11±0.07	21±11	4.1±1.7	0.02±0.01	24.6±12	-	0.18±0.1
Detection limit	0.1	0.2	0.8	0.1	0.3	0.8	0.03	0.003	0.003	0.04	0.001	0.0002	0.002	0.0000
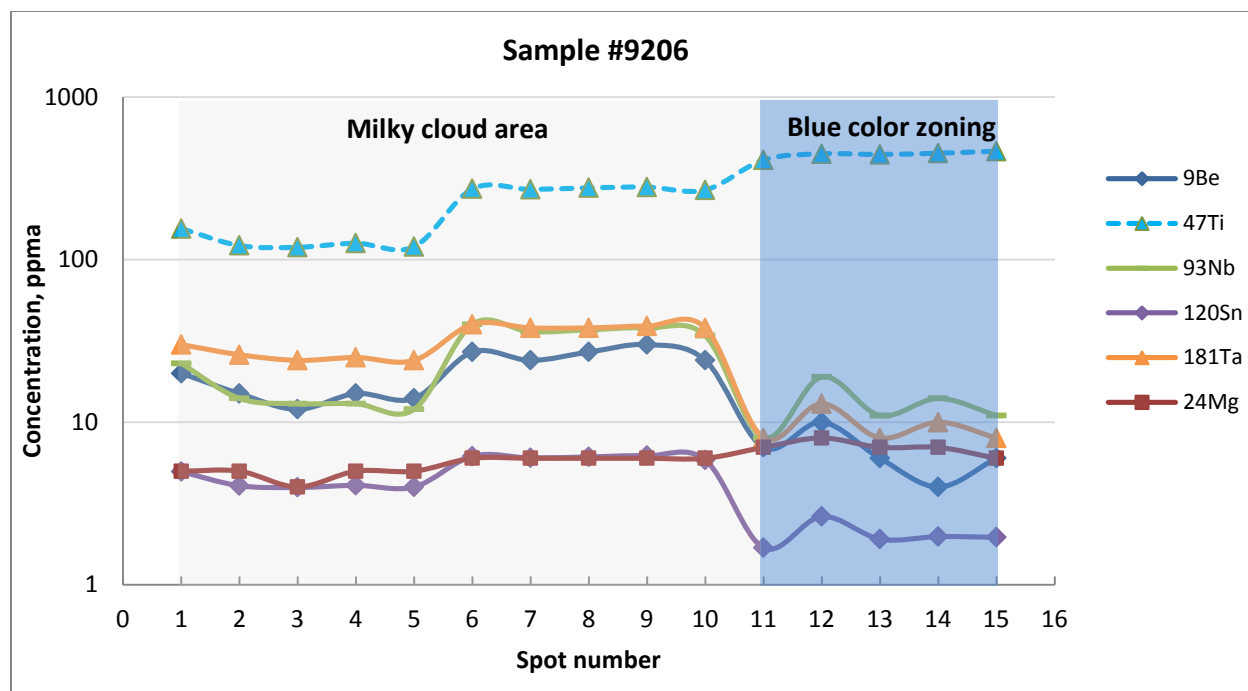
Figure 73: Correlation between laser spots and trace elements in different particle areas on GIA sample #9206 indicating natural Be in sapphire.

Sample #9206 showed different chemistry between areas of milky clouds and blue color zoning. Milky clouds contained higher amounts of Be which relate to Nb, Sn, Ta, and Th levels. The blue color zoning also showed similar chemistry, but higher amounts of Ti when compared with Be, Nb, Sn, Ta, and Th in areas of milky clouds, (see correlation in figure 73). It is interesting that the areas of milky clouds have lower amounts of Ti, but higher amounts of Be, which is different from sample #8102. This might be due to Be-bearing nano-inclusions hidden in areas of blue color zoning. However, advanced instrumentation such as high-resolution transmission electron microscopy (HRTEM) would be required to study this sample further.

Blue Sapphire of GIA sample #7122

GIA sample #7122 is a partial trapiche-like Pailin sapphire sample comprising a hexagonal-shape core area with radiating arms (figure 74). This sample had milky clouds and natural healed fractures. Chemical analysis showed following (see table 7).

Color calibrated using transmitted illumination

Dark field and fiber-optic illumination

Figure 74: GIA sample #7122-A showing the location of the 25 spots where LA-ICP-MS analysis was conducted on different areas. The photo was color calibrated and captured using transmitted light (left) and bright field and fiber-optic illumination (right). Photo: S. Engniwat © GIA.

Table 7: LA-ICP-MS results in parts per million atomic (ppma) units for GIA sample #7122.

GIA sample #7122 Spot number (color of the area)	9Be	24Mg	47Ti	51V	52Cr	55Mn	56Fe	69Ga	90Zr	93Nb	120Sn	178Hf	181Ta	182W	232Th
sp1 (Dense brown particles)	5	11	434	5	BDL	36	2957	57	0.51	74	3.06	0.03	45	0.03	0.66
sp2 (Dense brown particles)	8	9	131	4	BDL	11	2468	55	0.56	95	1.69	0.05	50	0.04	1.10
sp3 (Dense brown particles)	2	9	253	5	BDL	28	2629	58	0.32	47	1.69	0.03	25	0.02	0.64
sp4 (Dense brown particles)	2	12	245	5	BDL	29	2848	63	0.29	45	1.38	0.02	25	0.02	0.52
sp5 (Dense brown particles)	BQL	8	116	4	BDL	14	2297	56	0.22	55	0.93	0.02	31	0.02	0.63
sp6 (Dense brown particles)	3	10	443	5	BDL	41	2822	59	0.42	70	2.27	0.04	38	0.03	0.64
sp7 (Brown particles)	BQL	5	390	3	BDL	6	1964	46	0.03	0.57	0.73	BQL	0.31	BDL	0.04
sp8 (Brown particles)	BQL	5	384	3	BDL	24	2041	45	0.09	2.83	0.71	BQL	1.24	BDL	0.05
sp9 (Brown particles)	BQL	6	609	4	BDL	29	2304	50	0.08	2.72	0.87	BQL	1.23	BDL	0.04
sp10 (Brown particles)	BQL	5	253	3	BDL	10	2085	49	0.02	3.25	0.62	0.01	1.25	BDL	0.18
sp11 (Brown particles)	BQL	5	439	4	BDL	5	2191	48	0.05	4.54	1.17	0.01	2.32	BDL	0.03
sp12 (Blue)	BQL	4	328	3	BDL	0.5	2282	50	BDL	0.44	1.01	0.01	0.34	BDL	0.00
sp13 (Blue)	BDL	3	271	3	BDL	0.4	2242	51	0.02	0.34	0.78	BQL	0.25	BDL	BQL
sp14 (Blue)	BDL	3	176	3	BDL	BQL	1917	45	BDL	0.04	0.63	BQL	0.07	BDL	BQL
sp15 (Blue)	BDL	2	101	3	BDL	BQL	1877	41	BDL	0.12	0.17	BDL	0.03	BDL	BQL
sp16 (Blue)	BQL	3	230	3	BDL	0.6	1862	43	0.02	0.25	0.58	BQL	0.35	BDL	BQL
Average±SD	-	6±3	300±141	4±0.9	-	-	2299±356	51±6	-	25±33	1.1±0.7	-	14±19	-	-
Detection limit	0.5	0.1	0.1	0.1	0.8	0.1	5.0	0.07	0.004	0.01	0.04	0.001	0.0005	0.002	0.0003

The collected chemical data showed different chemistry depending on the area analyzed. All elements showed highest concentrations at the core or in areas with dense brown particles and trended to decrease in other areas. We only found Be content in areas with dense brown particles, which also correlated with manganese (Mn), tantalum (Ta), niobium (Nb), and thorium (Th) concentrations. We found small amounts of magnesium (Mg) and vanadium (V), but detected no Cr. The iron (Fe) content we obtained ranged widely from 1862 ppma in areas with blue coloration and up to 2957 ppma in areas with dense brown particles.

We consider it possible that all elements detected in areas with dense brown zones or brown particles are partially derived from inclusions enriched in these high field strength elements such as Nb, Ta. We have identified these inclusions as Fe-tapiolite, tantalite and hematite using Raman spectroscopy. In order to confirm the presence of this mineral, we need further analysis. Other heavy elements such as Zr, W, and Th, were also observed in relation with Be. These elements are commonly found in particle inclusions in natural sapphire.

3.3 Comparison between Pailin blue sapphire and other basalt-related sapphires

Basalt-related sapphires are an important part of the gemstone trade. Historically important sources are Cambodia and Thailand, while Australia is still producing large quantities of sapphire. Recent discoveries on the African continent in Nigeria and Ethiopia have added more basalt-related sapphires to the trade.

These stones remain some of the most challenging for origin determination and making the distinction between the various basalt-related sapphire sources is very complicated. Due to their similar geological formation which is still poorly understood, it is hard to single out discriminating characteristics. During this study, the newly collected data on the Pailin stones was compared to data from other stones in GIA's reference collection. A few interesting observations were made.

We found an interesting FTIR feature in 8 Pailin sapphires, which showed a higher peak height at 3232 cm^{-1} than the peak at 3309 cm^{-1}. This is summarized in table 8. This feature is found in blue sapphires from Nigeria, but had never been found in samples from Australia, Thailand or Ethiopia. We currently don't understand why this is the case and further analysis is required.

Table 8: Comparison of FTIR features in basalt –related blue sapphires from different localities.
Note: Kaolinite is commonly found. Some samples which showed no diagnostic features are not listed in this table.

Country	total sample number	single 3309 cm^{-1}	3309 series; where 3309 > 3232 cm^{-1}	3309 series; where 3309 ≤ 3232 cm^{-1}
Australia	42	9	33	-
Cambodia	48	2	33	10 (3309<3232)
Thailand	46	27	9	-
Nigeria	73	5	46	18 (3309≤3232)
Ethiopia	22	4	16	-

Chemical analysis using LA-ICP-MS is summarized in table 9. We separate results from areas sampled with no particles and those sampled from areas with particles or clouds. Samples from Pailin, Mambilla, New South Wales, Queensland, Tasmania and Ethiopia had areas with particles or cloud inclusions, whereas samples from Thailand, Ambondromifehy, Madagascar and Garba Tula, Kenya had very few samples with areas of particles. Therefore these results are reported as 'no particle' areas only. Most Pailin, Mambilla, Nigeria and Ethiopian sapphires contained lower amounts of Fe than sapphires from other localities. A plot between Fe/Ga and Mg/Ga is potentially useful to separate Pailin sapphire from other locaities (figure 75), even though there is overlap with some Nigerian and Ethiopian samples. Elements like Be, Mg, Ti, Nb, Sn, and Ta were present in higher amounts in areas with particle inclusions than samples with areas without particles. Samples from Pailin, Mambilla, Queensland, and Ethiopia showed very high amounts of Nb and Ta, including 62, 72, 85 and 162 ppma for Nb and 40, 103, 54 and 68 ppma for Ta, respectively. For Tasmania samples showed the highest amount of Sn in areas with particles (up to 26 ppma).
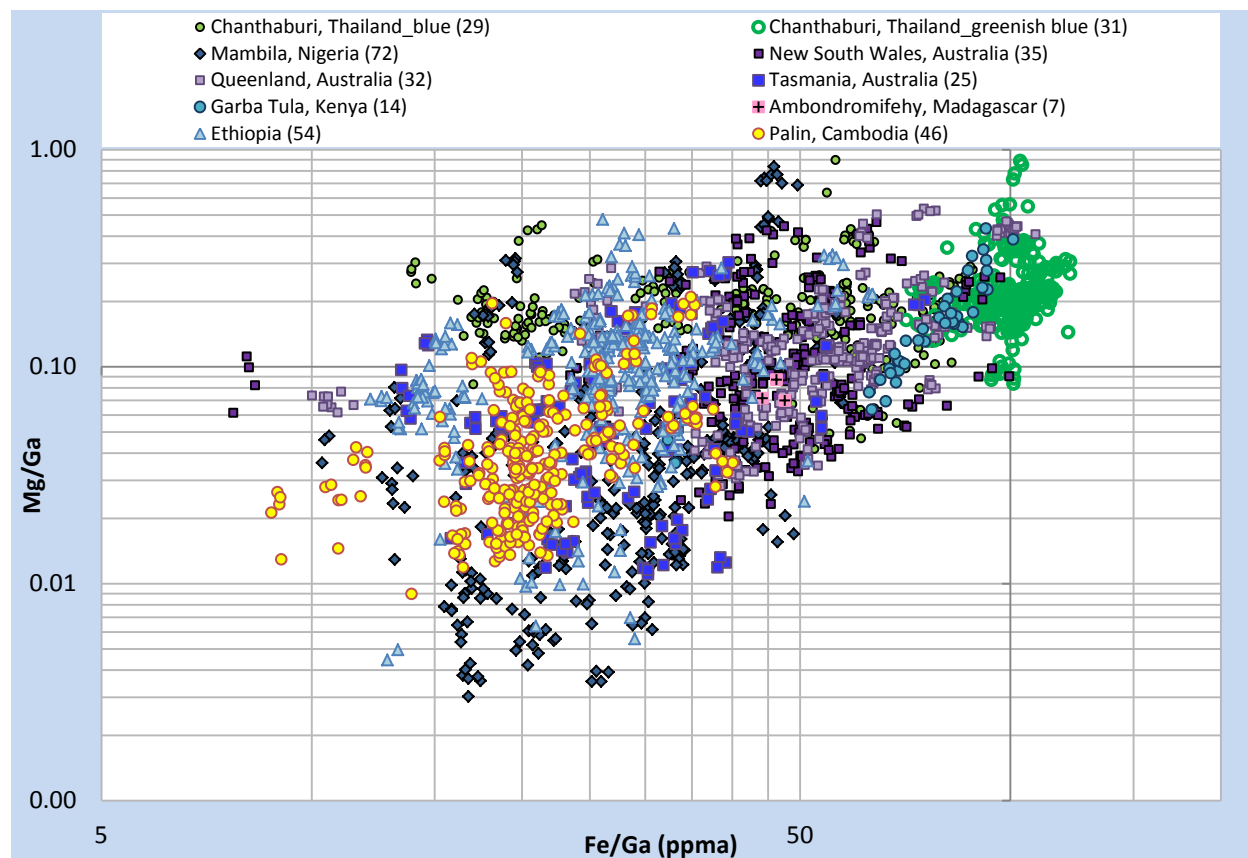
Figure 75: Plot showing Fe/Ga and Mg/Ga in sapphires from Pailin sapphires, compared to data from other basalt-related blue sapphire deposits in Australia, Nigeria, Thailand, and Ethiopia.

Table 9: Chemical data on alkali basalt blue sapphire from six different geographical localities using LAICPMS [Min-Max range (mean)]* in ppma or parts per million by atom.

Element	Pailin, Cambodia (n=55)		Mambilla, Nigeria (n=49)		New South Wales, Australia (n=35)		Queensland, Australia (n=34)		Tasmania, Australia (n=25)	
	No particles	Particles	No particles	Particles	No particles	Particles	No particles	Particles	No particles	Particles
^{9}Be	BDL-3 (BDL)	BDL-30 (2.63)	BDL-3 (BDL)	BDL-96 (5.7)	BDL-2.26 (BDL)	2.56-4.30 (3.6)	BDL-2.8 (BDL)	0.61-7.5 (2)	BDL-1.86 (BDL)	0.66-8.76 (3.0)
^{24}Mg	BDL-12 (1.5)	1-12 (4)	BDL-25 (BDL)	BDL-17 (BDL)	BDL-22 (3.9)	7-8 (7.6)	BDL-21 (4.6)	5-22 (16)	BDL-11 (1.7)	BDL-14 (3.1)
^{47}Ti	3-404 (49)	28-579 (155)	BDL-554 (34)	4-528 (182)	BDL-967 (58)	102-270 (164)	7-524 (41)	30-1316 (210)	BDL-520 (40)	2-304 (159)
^{51}V	2-15 (4)	2-22 (6)	BDL-11 (BDL)	BDL-5 (1.30)	BDL-9 (3±2)	5-5 (5)	2-10 (4.6)	4-8 (6)	BDL-5 (0.9)	BDL-3 (0.6)
^{53}Cr	2-13 (BDL)	1-5 (BDL)	BDL-33 (BDL)	BDL-20 (BDL)	BDL-19 (3.1)	BDL	BDL-22 (BDL)	BDL-18 (BDL)	BDL-11 (BDL)	BDL-8 (BDL)
^{57}Fe	529-2005 (991)	657-3761 (1136)	628-2961 (1030)	876-1329 (1052)	789-3870 (2241)	1862-1997 (1953)	716-3688 (2176)	1460-4893 (2861)	986-2987 (1407)	1070-2183 (1479)
^{69}Ga	30-92 (51)	36-128 (56)	27-91 (47)	27-110 (55)	27-113 (46)	49-50 (49)	30-79 (42)	40-59 (49)	30-101 (50)	40-98 (58)
^{93}Nb	BDL-2.52 (0.01)	BDL-62 (1.76)	BDL-1.56 (BDL)	0.02-72 (1.04)	BDL-0.64 (BDL)	0.24-1.67 (0.8)	BDL-1.91 (BDL)	BDL-85 (0.46)	BDL-0.93 (BDL)	0.19-7.22 (1.03)
^{120}Sn	0.09-0.71 (BDL)	0.11-6 (0.43)	BDL-3.9 (0.13)	BDL-3.6 (0.38)	BDL-4.3 (BDL)	0.70-1.17 (0.84)	BDL-2.37 (BDL)	BDL-8 (0.95)	BDL-11 (0.65)	BDL-26 (7.2)
^{181}Ta	BDL-4.15 (0.04)	0.01-40 (4.06)	BDL -3.31 (0.05)	0.12-103 (5.54)	BDL-1.33 (0.01)	2.63-8.98 (5.73)	0.00-4.73 (BDL)	0.34-54 (0.80)	BDL-7.22 (0.12)	0.81-9.05 (3.7)

http://www.gia.edu

Element	Ethiopia (n=46)		Chanthaburi, Thailand (blue); (n=29)	Chanthaburi, Thailand (greenish blue, n=31)	Ambondromifehy, Madagascar (n=7)	Garba Tula, Kenya (n=14)	Detection limit
	No particles	Particles					
^{9}Be	BDL-2.09 (BDL)	0.7-70 (3.8)	BDL-0.79 (BDL)	BDL-0.93 (BDL)	BDL-9 (BDL)	BDL	0.46
^{24}Mg	BDL-18 (4)	5-12 (6.8)	2-33 (7)	3-50 (8)	BDL-5 (BDL)	2-73 (6)	0.06
^{47}Ti	4-379 (35)	24-507 (120)	9-159 (33)	5-91 (21)	3-386 (12)	8-31 (13)	0.41
^{51}V	BDL-13 (5)	1-6 (1.3)	1-23 (5)	BDL-2 (0.71)	0-1 (BDL)	BDL-0.90 (BDL)	0.04
^{53}Cr	BDL-4 (BDL)	BDL	BDL-53 (1.5)	BDL-11 (BDL)	BDL	BDL	0.60
^{57}Fe	825-2329 (1110)	989-1267 (1099)	675-2987 (1888)	2406-4966 (3727)	1176-2490 (1552)	1822-3487 (2967)	0.86
^{69}Ga	30-106 (36)	37-80 (73)	32-57 (38)	27-54 (37)	27-59 (53)	33-81 (39)	0.02
^{93}Nb	BDL-2.01 (BDL)	BDL-162 (0.37)	BDL-0.15 (BDL)	BDL-0.01 (BDL)	BDL-1.54 (BDL)	BDL	0.001
^{120}Sn	BDL-1.19 (BDL)	BDL-0.57 (BDL)	BDL-0.39 (BDL)	BDL-0.14 (BDL)	BDL-6.22 (BDL)	BDL	0.001
^{181}Ta	BDL-2.47 (BDL)	BDL-68 (0.61)	BDL-0.32 (BDL)	BDL-0.02 (BDL)	BDL-7.46 (0.02)	BDL	0.001

http://www.gia.edu

PART IV: SUMMARY

Basalt-related sapphires are an important part of the trade with deposits that have been, and still are, producing vast amounts of blue sapphires in all qualities. Historically important sources are Cambodia and Thailand, while Australia is still producing large quantities of sapphire. Recent discoveries on the African continent in Nigeria and Ethiopia have added more basalt-related sapphires to the trade. Even though these stones are found in completely different localities all around the world, they all show similar characteristics because they formed in geologically similar environments.

Most sapphires from Pailin, Cambodia have milky inclusions and intersecting growth tubes along twinning. Melted inclusions associated with decrepitation haloes were common seen, similar to sapphires from other alkali-basalt deposits. The milky inclusions in Pailin sapphires are most similar to those in sapphires from Mambilla, Nigeria (Pardieu 2014). However, Nigerian sapphires contained richer milky inclusions which are associated with colorless and often brown zoning depending on the density of particles. Streamers or flake-like inclusions are similar to those observed in sapphires from Vietnam, Nigeria and Australia (Smith 1995, Pardieu 2014). Other inclusions, such as partially healed fissures, tiny inclusions associated with decrepitation haloes or mineral inclusions (pyrochlore, feldspar, and zircon) were commonly seen in all alkali sapphires. As we observed pyrochlore in Australia, and Nigerian samples in our collections. We also found many localities producing trapiche-like sapphire, including Pailin. These have very similar brown particle inclusions and chemistry.

After these authors have studied different sources of alkali basalt-related blue sapphires, we know it is challenging to give origin determination without a combination of microscope and advanced instrumentation, especially chemistry or LA-ICP-MS. Analysis of specific areas of inclusions can be helpful for origin determination.

ABOUT THE AUTHORS. Sudarat Saeseaw (ssaeseaw@gia.edu) is senior manager of colored stone identification in GIA's Bangkok laboratory. Dr. Supharart Sangsawong is a former research scientist in GIA, currently working as gemstone testing manager at the Bahrain Institute for Pearls & Gemstones (Danat). Wim Vertriest (wvertrie@gia.edu) is a field gemologist at GIA's Bangkok laboratory. Ungkhana Atikarnsakul (uatikarn@gia.edu) is an analyst technician at GIA's Bangkok laboratory.

PART V. BIBLIOGRAPHY

Aspen, P., Upton, B. G. J. & Dickin, A. P. (1990). "Anorthoclase, sanidine and associated megacrysts in Scottish alkali basalts: high-pressure syenitic debris from upper mantle sources?" European Journal of Mineralogy 2, 503–517.

Baldwin, L. C., F. Tomaschek, C. Ballhaus, A. Gerdes, R. O. C. Fonseca, R. Wirth, T. Geisler and T. Nagel (2017). "Petrogenesis of alkaline basalt-hosted sapphire megacrysts. Petrological and geochemical investigations of in situ sapphire occurrences from the Siebengebirge Volcanic Field, Germany." Contributions to Mineralogy and Petrology **172**(6): 43.

Beran, A., Rossman, G.R., (2006). "OH in naturally occurring corundum." European Journal of Mineralogy **Vol.18**: pp. 441-447.

Berrangé J. P., Jobbins E. A. (1976) "The Geology, Gemmology, Mining Methods and Economic Potential of the Pailin Ruby and Sapphire Gem-field, Khmer Republic." Institute of Geological Sciences, Report No. 35.

Emmett, J. L., K. V. Scarratt, et al. (2003). "Beryllium diffusion of ruby and sapphire." Gems & Gemology **Vol. 39**(No. 2, Summer): pp. 84–135.

Ferguson, J. and P. E. Fielding (1971). "The origins of the colours of yellow, green, and blue sapphires." Chemical Physics Letters. **Vol. 10**: pp. 262, 265.

Fritsch, E. and M. Mercer (1993). "Blue color in sapphire caused by Fe^{2+}/Fe^{3+} intervalence charge transfer [letter to the editor]." Gems & Gemology **Vol. 29**(No. 3, Fall): pp. 151, 226.

Gübelin, E. J. and J. I. Koivula (1986). Photoatlas of Inclusions in Gemstones. Zürich, Switzerland, ABC Edition.

Hughes, R. W. (1997). Ruby & Sapphire. Boulder, CO, RWH Publishing.

Jingfeng Guo, S. Y. O'Reilly, et al. (1996). "Corundum from basaltic terrains: A mineral inclusion approach to the enigma." Contributions to Mineralogy and Petrology. **Vol. 122**: pp. 368–386.

Jobbins E. A., Berrangé J. P. (1981) "The Pailin Ruby and Sapphire Gemfield, Cambodia" Journal of Gemmology, Vol. 17 (No.8, Oct.): pp. 555–567.

Keller, P. C. (1982). "The Chanthaburi-Trat gem field, Thailand." Gems & Gemology **Vol. 18**(No. 4, Winter): pp. 186–196.

Levinson, A. A. and F. A. Cook (1994). "Gem corundum in alkali basalt: Origin and occurrence." Gems and Gemology **30** (4): 253-262.

Ma Huan (1970). Ying-Yai Sheng-Lan 'The overall survey of the ocean's shores' [1433]. Cambridge, Hakluyt Society.

Pardieu, V. (2007). "Discovering beryllium in Madagascar blue sapphires." InColor Magazine.

Pardieu, V. (2009). "Concise Field Report. Volume 1: Pailin, Cambodia (Dec 2008 – Feb 2009)." from http://www.giathai.net/pdf/Public_Report_PR01_Pailin.pdf.

Pardieu, V. (2013). "Blue Sapphires and Beryllium: An Unfinished World Quest." InColor(No 23): pp. 36–43.

Pardieu, V., Saewseaw, S., Thirangoon, K., Lomthong, P., (2011). "Beryllium- and Tungsten-Bearing Sapphires from Afghanistan." Gems & Gemology **Vol. 47**(Spring 2011): 53-54.

Pardieu, V., Sangsawong, S., Muyal, J., Sturman, N., (2014). "New Nigerian Source of Blue Sapphire." https://www.gia.edu/gia-news-research-nigerian-source-blue-sapphire

Shen, A., Lu, R. (2011). "Unusually High Beryllium in Three Blue Sapphires." Gems & Gemology **Vol. 47**(No 3): pp 232-233.

Saminpanya, S. and F. L. Sutherland (2011). "Different origins of Thai area sapphire and ruby, derived from mineral inclusions and co-existing minerals." European Journal of Mineralogy **23**(4): 683-694.

Shen, A., McClure S., Breeding C. M., Scarratt K., Wang W., Smith C., Shigley J. (2007). Beryllium in Corundum: The Consequences for Blue Sapphire. . GIA Insider. January 26.

Shen, A., Wirth, R., (2012). "Beryllium-bearing nano-inclusions identified in untreated Madagascar sapphire." Gems & Gemology **Vol. 48**(No. 2): 150-151.

Smith, C. P. (1995). "A contribution to understanding the infrared spectra of rubies from Mong Hsu, Myanmar." Journal of Gemmology **Vol. 24**(No. 5, Jan.): pp. 321–335.

Smith, C. P., Kammerling, R.C., Keller, A.S., Peretti, A., Scarratt, K.V., Khoa, N.D., Repetto, S., (1995). "Sapphires from southern Vietnam." Gems & Gemology **Vol. 31**(No. 3, Fall): pp. 168–186.

Sutherland, F. L., G. Giuliani, et al. (2009). "Sapphire-ruby characteristics, west Pailin, Cambodia." Australian Gemmologist **Vol. 23**(No. 1): pp. 401–406.

Sutherland, F. L., P. W. O. Hoskin, C. M. Fanning and R. R. Coenraads (1998). "Models of corundum origin from alkali basalt terrains: A reappraisal." Contributions to Mineralogy and Petrology **133**(4): 356-372.

Vichit, P., S. Vudhichativanich and R. Hansawek (1978). "The distribution and some characteristics of corundum-bearing basalts in Thailand." Journal of the Geological Society of Thailand **Vol. 3**: pp. M4–1 to M4–38.

Wathanakul, P., Atichat, W., Pisutha-Arnond, V., Win, T.T., Singbamrung, S. (2004). Evidence of the unusually high Be, Sn, Nb, Ta content in some trapiche like sapphires from basaltic origin. 29th International Gemmological Conference, Wuhan , China.